RSC Advances

PAPER

View Article Online
View Journal | View Issue

Cite this: *RSC Adv.*, 2025, **15**, 20061

Combined antimicrobial and anti-inflammatory properties of electrospun PCL nanohybrids infused with metal-turmeric oleoresin and metal-curcuminoids†

Dinithi Senanayake, [a] Piumika Yapa, [a] Sanduni Dabare, [a] Imalka Munaweera, *[a] Manjula M. Weerasekera, [b] Thusitha N. B. Etampawala, [cd] Maheshika Sethunga, [e] Dinesh Attygalle [f] and Shantha Amarasinghe [f]

The increasing risk of microbial infections and antimicrobial resistance requires the development of sustainable biomaterials with improved therapeutic properties for effective and environmentally friendly health and safety applications, leading to the exploration of advanced multifunctional nanomaterials. This study introduces a novel electrospun polymeric membrane that integrates a trimetallic nanohybrid composed of silver (Ag), copper (Cu), and nickel (Ni) with curcuminoids derived from turmeric oleoresin. This combination is incorporated into a biodegradable polycaprolactone (PCL) electrospun mat. The synthesis and characterization of the nanohybrids were performed using Fourier-transform infrared spectroscopy (FTIR), Raman spectroscopy, X-ray diffraction (XRD), scanning electron microscopy (SEM), and UV diffuse reflectance spectrometry. The electrospun membranes incorporated with a trimetallic and curcuminoids nanohybrid demonstrated a synergistic antimicrobial effect, as evidenced by inhibition zones measuring between 29.67 ± 0.24 and 33.17 ± 0.24 mm against a wide range of bacterial and fungal strains. The primary antimicrobial mechanism is attributed to radical scavenging activity (RSA), which reached a maximum value of 76.14 ± 0.99% in the trimetallic and curcuminoids nanohybrid incorporated PCL mat. Furthermore, the curcuminoids displayed significant anti-inflammatory effects, achieving a maximum reduction of 72.81 ± 0.33% at a concentration of 5000 ppm. The electrospun membranes effectively reduce microbial growth, are biodegradable, non-toxic, pose minimal hazards, and are environmentally friendly, aligning with sustainable technologies for biomedical applications. These membranes function as physical and biological barriers, offering an eco-conscious, cost-effective alternative to conventional antimicrobial strategies. This research highlights the potential of trimetallic–curcuminoid nanohybrid electrospun membranes as sustainable biomaterials for advanced antimicrobial treatments, contributing to safer and more effective biomedical applications while ensuring biocompatibility and environmental safety. It exemplifies how innovative solutions can tackle health and sustainability challenges.

Received 7th March 2025
Accepted 1st June 2025

DOI: 10.1039/d5ra01642h

rsc.li/rsc-advances

1 Introduction

Electrospun nanofiber systems incorporating organic–inorganic nanohybrids have gained increasing attention in biomedical sciences due to their multifunctionality, structural versatility, and ability to integrate bioactive components for enhanced therapeutic performance.[1,2] These systems are capable of replicating the extracellular matrix, facilitating cell attachment and proliferation, while allowing for the controlled release of incorporated agents. Polycaprolactone (PCL),

[a]*Department of Chemistry, Faculty of Applied Sciences, University of Sri Jayewardenepura, Nugegoda 10250, Sri Lanka. E-mail: imalka@sjp.ac.lk; dinithisenanayake3@gmail.com; piumikayapa@gmail.com; dabaresanduni@gmail.com; Tel: +94 772943738*

[b]*Department of Microbiology, Faculty of Medical Sciences, University of Sri Jayewardenepura, Nugegoda 10250, Sri Lanka. E-mail: mmweera@sjp.ac.lk*

[c]*Department of Polymer Science, Faculty of Applied Sciences, University of Sri Jayewardenepura, Nugegoda 10250, Sri Lanka*

[d]*Center for Nanocomposite Research, Faculty of Applied Sciences, University of Sri Jayewardenepura, Nugegoda 10250, Sri Lanka. E-mail: tetampa@sjp.ac.lk*

[e]*Department of Food Science and Technology, University of Sri Jayewardenepura, Nugegoda 10250, Sri Lanka. E-mail: maheshichathuranganee@gmail.com*

[f]*Department of Material Science and Engineering, Faculty of Engineering, University of Moratuwa, Sri Lanka. E-mail: dattyga@uom.lk; amarasinghes@uom.lk*

† Electronic supplementary information (ESI) available. See DOI: https://doi.org/10.1039/d5ra01642h

a biodegradable and biocompatible polymer, is widely utilized in electrospinning due to its excellent mechanical properties, slow degradation rate, and compatibility with a broad range of bioactive molecules.[3,4] These attributes make PCL-based electrospun mats ideal platforms for wound healing and antimicrobial applications.

Metal nanoparticles (MNPs) such as silver (Ag), copper (Cu), and nickel (Ni) are widely recognized for their potent antimicrobial properties across a broad spectrum of pathogens, including antibiotic-resistant strains.[5,6] Their mechanisms include disruption of microbial membranes, induction of reactive oxygen species (ROS), DNA and protein interaction, and oxidative stress.[7,8] Notably, combining different MNPs into trimetallic systems has demonstrated synergistic effects that enhance antimicrobial activity while reducing the dosage and cytotoxicity typically associated with single-metal nanoparticles.[9,10] Garza-Cervantes *et al.*[10] highlighted how the co-incorporation of Ag with Cu and Ni significantly improved antimicrobial efficacy while maintaining low toxicity towards human cells. Similarly, nanohybrids comprising CuO, ZnO, and WO_3 showed over 90% higher antimicrobial activity than their monometallic counterparts, attributed to increased lipid peroxidation and membrane damage.[11]

To further enhance therapeutic efficiency, natural bioactive compounds such as curcumin; an active polyphenol in turmeric, have been integrated into nanofiber systems. Curcumin is known for its broad-spectrum antibacterial activity, with efficacy against both gram-positive and gram-negative bacteria, including resistant strains such as *Staphylococcus aureus* and *Escherichia coli*.[12] In addition to its antimicrobial properties, curcumin exhibits strong antioxidant and anti-inflammatory activities, making it a highly versatile therapeutic agent.[13,14] However, its clinical application is limited by low aqueous solubility, rapid metabolism, and poor bioavailability.[15] To overcome these limitations, curcumin has been combined with metal nanoparticles and embedded into electrospun nanofibers or encapsulated within nanocarriers, improving its stability, solubility, and biological performance.[16–18]

In this study, rather than using isolated curcumin, we chose to extract curcuminoids from turmeric oleoresin, a natural extract containing a broader spectrum of turmeric-derived bioactives. Turmeric oleoresin is obtained during curcumin production and contains a mixture of curcumin, demethoxycurcumin, bisdemethoxycurcumin, and essential oils.[13,14] This full-spectrum composition offers unique advantages over pure curcumin. First, it exhibits enhanced biological synergy, as the combination of curcuminoids and essential oils can lead to stronger antioxidant and anti-inflammatory responses.[19,20] Second, turmeric oleoresin has been shown to activate cannabinoid receptor 2 (CBR2), mediating potent anti-inflammatory effects in osteoarthritis models.[19] Third, the essential oil fraction enhances membrane permeability and improves the solubility of curcuminoids in hydrophobic polymer matrices such as PCL, facilitating uniform distribution and release.[20] Furthermore, the extraction of curcuminoids from turmeric oleoresin aligns with green chemistry and sustainability goals, utilizing a low-waste, cost-effective process that avoids synthetic derivatization. These characteristics make turmeric oleoresin a valuable and underutilized source of bioactive compounds for biomedical applications.

Despite the widespread use of curcumin in electrospun nanofiber research, very few studies have investigated turmeric oleoresin-derived curcuminoids in this context. Moreover, most existing studies focus on single-metal nanoparticles, with limited exploration of trimetallic systems such as Ag–Cu–Ni, particularly in combination with natural polyphenols. This study addresses these gaps by formulating and characterizing a novel electrospun PCL membrane that integrates curcuminoids extracted from turmeric oleoresin and a trimetallic nanohybrid of Ag, Cu, and Ni. The goal is to harness the synergistic antibacterial, antioxidant, and anti-inflammatory effects of this hybrid system for potential biomedical use.

Electrospinning offers a scalable and cost-effective method for fabricating such multifunctional membranes. It enables the incorporation of a wide range of antimicrobial agents; including metal nanoparticles, natural polyphenols, and antibiotics; into diverse polymer matrices.[21–23] These nanofibers provide not only high surface area and porosity but also allow sustained and controlled release of active compounds. The method also supports advanced configurations such as coaxial and multilayered structures, enabling further functionalization.[24] Mechanical strength, thermal stability, and tunable degradation profiles can be achieved through blending and adjusting processing parameters, making electrospun membranes suitable for demanding clinical environments.[25,26]

Natural antimicrobials embedded in electrospun fibers, such as those from turmeric, can effectively prevent infection, modulate inflammation, and promote healing. Curcumin and related curcuminoids have been shown to reduce inflammation, scavenge free radicals, and support collagen synthesis and re-epithelialization; key processes in wound healing.[12,13,20] When combined with metals in a nanohybrid form, these bioactives exhibit enhanced therapeutic efficacy due to improved cellular uptake and ROS generation.[16–18] Importantly, the use of biodegradable, biocompatible components such as PCL, oleoresin, and essential trace metals ensures environmental safety and long-term sustainability; addressing the critical global need for antimicrobial solutions that avoid contributing to resistance and pollution.[27,28]

This study (Fig. 1) introduces an innovative electrospun polymeric membrane that incorporates three metals (Ag, Cu, Ni) alongside curcuminoids derived from turmeric. This multifaceted approach aims to combat microbial growth while prioritizing environmental sustainability. By utilizing biodegradable materials and natural compounds, this membrane shows significant potential as a sustainable alternative for medical and safety-related applications. The system is comprehensively characterized using Fourier-transform infrared spectroscopy (FTIR), Raman spectroscopy, X-ray diffraction (XRD), scanning electron microscopy (SEM), and UV diffuse reflectance spectrometry (UV-DRS). Functional assessments include antimicrobial zone-of-inhibition studies, radical scavenging activity (RSA), and anti-inflammatory testing. The results demonstrate that this system functions effectively as

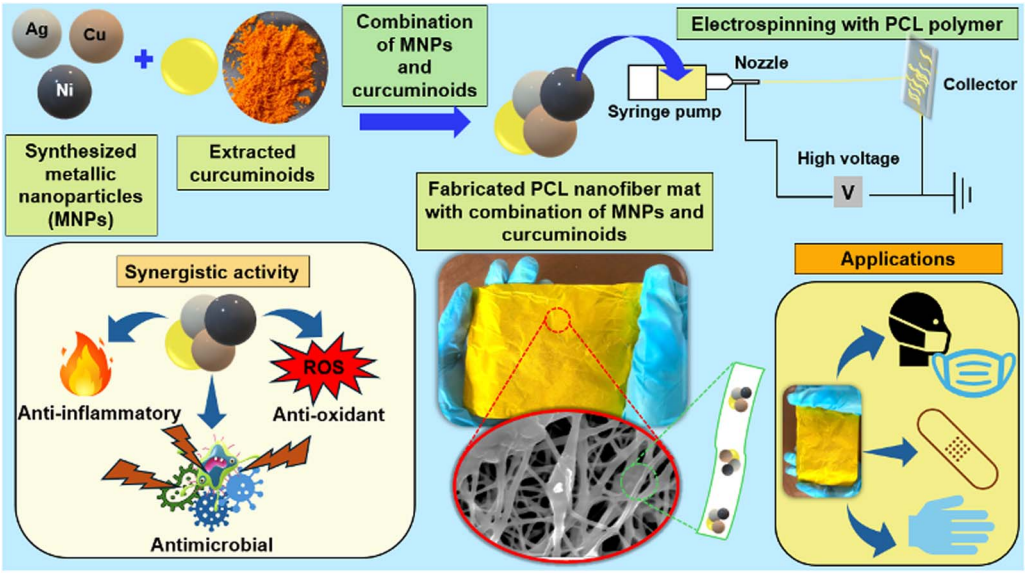

Fig. 1 A graphical illustration of the research approach.

a physical and biological barrier, offering a sustainable, multi-functional solution for antimicrobial and wound healing applications. By combining the strengths of natural and synthetic agents, the presented nanohybrid platform aligns with the dual imperatives of clinical performance and environmental stewardship.

Furthermore, the developed membrane, based on PCL (polycaprolactone), combines Ag, Cu, and Ni metal nanoparticles with curcuminoids. The combination of these components into a single material creates a powerful synergistic effect, providing antimicrobial, antioxidant, and anti-inflammatory benefits, making it effective against resistant strains and a broad spectrum of microbes. The incorporation of these nanohybrids into PCL membranes ensures their availability, affordability, and cost-effectiveness while functioning as both a physical and biological barrier. This multi-functionality is especially important in wound care, where preventing infection and reducing inflammation are crucial for effective healing. Additionally, using biodegradable and biocompatible materials not only improves the solution's effectiveness but also highlights a commitment to sustainability and environmental responsibility. This innovative approach has the potential to significantly enhance health and safety outcomes while addressing important sustainability challenges.

2 Materials and methods

2.1 Materials and reagents

All reagents and other chemicals, including silver nitrate, copper sulphate, nickel chloride, ascorbic acid, sodium borohydride, ethanol, methanol, acetone, ethyl acetate, chloroform, dimethyl sulfoxide, 2,2-diphenyl-1-picrylhydrazyl, and polycaprolactone ($M_n = 80\,000$) were purchased from Sigma Aldrich in the United States. Additionally, the chemicals, media, and other materials required for microbiology research, such as nutritional agar, Muller Hinton agar, bacteriological agar, Sabourauds dextrose agar, blood agar, and antibiotic powders, were obtained from HiMedia in India. All the chemicals were of analytical grade.

For microbiology studies, the bacterial strains, including *Staphylococcus aureus*, MRSA, *Escherichia coli*, and *Pseudomonas aeruginosa,* along with the ATCC fungal strain of *Candida albicans* (ATCC 10231) were obtained from the Department of Microbiology, University of Sri Jayewardenepura, Sri Lanka.

Dried turmeric (*Curcuma longa*) slices were procured from a supplier in the northwestern province of Sri Lanka. Reference curcuminoids were purchased from Sigma Aldrich, USA.

2.2 Methodology

2.2.1 Extraction, purification, and characterization of turmeric oleoresin and purification of curcuminoids from dried turmeric (*Curcuma longa*) slices

2.2.1.1 Extraction of turmeric oleoresin from dried turmeric (Curcuma longa) slices. First, the moisture content of the dried turmeric slices was analyzed using a moisture analyzer. Then, dried turmeric slices were crushed and oleoresin was extracted using ethyl acetate as the solvent by the Soxhlet extraction method. The extraction process was conducted with a herb-to-solvent ratio of 1 : 10 for a duration of 10 to 12 hours.[29]

The extracts were filtered using Whatman No. 1 filter paper into a pre-weighed round-bottom flask. The solvent was then evaporated at 50 °C using a rotary evaporator. Afterwards, the oleoresin was dissolved in ethanol at a ratio of 1 : 10 (W/V) and heated to 50 °C until fully dissolved. The hot solution was filtered, and the filtration was cooled using an ice bath until crystals were formed.[30] Final and intermediate products were stored in a refrigerator at 4 °C in the dark until further analysis.

The crystalline structure of curcuminoids was determined using X-ray diffractograms (XRD). Data were acquired using

a Rigaku Ultima IV diffractometer equipped with a 3 kW sealed X-ray tube, operated at 40 kV and 30 mA, over a 2θ range of 5° to 50° at a scan rate of 1° min^{-1} with a 0.002° step width. To analyze the functional groups associated with the relevant peaks of curcuminoids and oleoresin, Fourier Transform Infrared (FTIR) analysis was performed using the KBr pellet method on a Bruker Vertex 80 instrument, across a range of 400 cm^{-1} to 4000 cm^{-1}. Identification and quantification of turmeric oleoresin and curcuminoids were carried out using thin-layer chromatography (TLC) and UV-vis spectrometric analysis, respectively.

The extracted oleoresin and purified curcuminoids crystals were analyzed using thin-layer chromatography (TLC) to identify the presence of various compounds in curcuminoids. The samples were prepared by applying reference curcuminoids, which were dissolved in methanol, onto two separate TLC plates. The plates were then placed in a pre-saturated chromatographic tank containing a solvent mixture of chloroform: methanol in a 95 : 5 ratio.[31] After allowing the chromatograms to air dry, the spots were observed using UV light. The retention factor (Rf) values were calculated using the following formula:

$$\text{Rf value} = \text{distance travelled by the spot/distance travelled by the solvent front}$$

Fig. S1† explains the method of quantification of oleoresin and Curcuminoids crystals by UV-vis spectrometric analysis.

2.2.2 Evaluation of anti-inflammatory activity of curcuminoids using egg albumin denaturation assay

2.2.2.1 Egg albumin separation for protein denaturation assay. The egg whites were separated from the yolks. A 25 mL portion of egg whites was measured and diluted with distilled water (1 : 1 ratio) to prepare a 100 mL solution. The solution was thoroughly mixed and stirred vigorously until the volume of the whitish substance visibly decreased. The resulting egg white solution was then subjected to centrifugation at 4000 rpm for 20 minutes. After centrifugation, the precipitated globulin was removed, leaving behind the egg albumin solution, which was used for the subsequent albumin denaturation assay.[32] ESI 1† explains the method of preparation of the samples.[33]

$$\text{Percentage inhibition} = \frac{A_c - (A_s - A_0)}{A_c} \times 100\%$$

A_c, A_s, and A_0 represent the respective absorbance of negative control, absorbance of sample after heating, and absorbance of the sample before heating at 680 nm wavelength.

2.2.3 Synthesis of Ag, Cu, and Ni metallic nanoparticles. Silver nitrate ($AgNO_3$), copper sulphate ($CuSO_4$), and nickel chloride ($NiCl_2$) were used as metal salt precursors to synthesize silver (Ag), copper (Cu), and nickel (Ni) nanoparticles *via* the chemical reduction method. A 50 mL solution of each metal salt (1 M) was prepared and stirred for 30 minutes at 80 °C at a speed of 800 rpm. For the reduction process, 60 mL of 1 M sodium borohydride ($NaBH_4$) was added dropwise to the $AgNO_3$ solution, while 60 mL of 2 M $NaBH_4$ was added dropwise to the $CuSO_4$ and $NiCl_2$ solutions, ensuring continuous stirring. After about 5 minutes, 60 mL of ascorbic acid (1 M for Ag and 2 M for Cu and Ni) was introduced as a capping agent. The resulting mixtures were continuously stirred for about 1 hour at 80 °C and maintained at 800 rpm. After the stirring process, the solutions were centrifuged at 4000 rpm for 20 minutes. The precipitates obtained were washed three times with a mixture of ethanol and distilled water in a 1 : 1 ratio, and then oven-dried until completely desiccated.[34,35]

To evaluate the synergistic activities of metallic nanoparticles, each nanoparticle (monometallic nanohybrid) was combined in equal proportions to form bimetallic and trimetallic nanohybrids, allowing for a comparative study of their enhanced properties.

2.2.4 Characterization of synthesized metallic nanoparticles. The characterization of the synthesized metallic nanoparticles was conducted by using many analytical techniques such as FTIR, XRD, SEM, EDAX, and UV-vis diffuse reflectance spectrometry. ESI 2† explains in detail this characterization.[36]

2.2.5 Particle size analysis and zeta potential for trimetallic nanoparticle combination. The same amount of all three metals (Ag, Cu, and Ni) was mixed together and ground well using a mortar and pestle, in order to form a fine powder. Then the mixture was dissolved in water, and it was ultrasonicated to get a homogeneous suspension. The particle size and zeta potential for the suspension of trimetallic nanoparticle combination were evaluated using Malvern Zetasizer Nano ZS Particle Size Analyser. Here, a 633 nm red laser passes through the particle suspension during the measurement and scattered light is detected and collected by a photo detector at a fixed scattering angle of 173°. All the measurements were conducted at room temperature.

2.2.6 Evaluation of antimicrobial efficacy (MIC, MBC, and IC_{50}) of metallic nanohybrids combined with curcuminoids and turmeric oleoresin. A promising approach to enhance antimicrobial efficacy involves combining metallic nanohybrids with curcuminoids and turmeric oleoresin. Bi- and tri-metallic nanohybrids were formulated by mechanochemical grinding of Ag, Cu, and Ni nanoparticles. These nanoparticles were blended to create various formulations, as detailed in Table 1, and combined with turmeric oleoresin and curcuminoids. In total, 23 test samples were created.

Stock solutions of nanoparticles, oleoresin, and curcuminoids were prepared and diluted to obtain working solutions at relevant concentrations for the study. To ensure the consistent nanoparticle suspensions, ultrasonication was employed prior to conducting the assays.

2.2.6.1 Antimicrobial testing. Minimum Inhibitory Concentration (MIC): MIC values were determined using a microdilution method in 96-well plates. Two-fold serial dilutions of nanoparticle suspensions were prepared, ranging from 10.00 mg mL^{-1} to 0.018 μg mL^{-1}. Microbial inocula were added to each well, and the plates were incubated for 24 hours at 37 °C. The MIC was evaluated using a colorimetric assay with resazurin dye. In this assay, the blue dye is reduced to a pink color by live microorganisms, indicating the presence of viable microbial cells.[37] Therefore, MIC was identified as the lowest

Table 1 Different nanoparticles blended formulations

Category	Composition
Monometallic	Ag, Cu, Ni
Bimetallic nanohybrid	Ag + Cu, Ag + Ni, Cu + Ni
Trimetallic nanohybrid	Ag + Cu + Ni
Oleoresin combinations	Ag + turmeric oleoresin, Cu + turmeric oleoresin, Ni + turmeric oleoresin, Ag + Cu + turmeric oleoresin, Ag + Ni + turmeric oleoresin, Cu + Ni + turmeric oleoresin, Ag + Cu + Ni + turmeric oleoresin
Curcuminoid combinations	Ag + curcuminoids, Cu + curcuminoids, Ni + curcuminoids, Ag + Cu + curcuminoids, Ag + Ni + curcuminoids, Cu + Ni + curcuminoids, Ag + Cu + Ni + curcuminoids
Only	Oleoresin, curcuminoids

concentration of the nanohybrid at which the dye began to change from blue to pink.

Following the evaluation of MIC, Minimum Bactericidal Concentration (MBC) and Minimum Fungicidal Concentration (MFC) were recorded as the lowest concentration at which no visible microbial growth was observed.

Inhibitory Concentration 50 (IC_{50}): the IC_{50} values were obtained through turbidimetric analysis. The optical density (OD) of microbial growth in the presence of varying concentrations of the nanohybrid was measured using an ELISA plate reader at 570 nm.[38] A dose–response curve was generated, and the IC_{50} value was determined as the concentration at which 50% growth inhibition occurred, utilizing GraphPad Prism software.

2.2.7 Well-diffusion assay of metallic nanoparticles combined with curcuminoids and turmeric oleoresins. To investigate the antimicrobial activity of metallic nanoparticles and their combinations, a well-diffusion assay was conducted. A total of 23 samples were tested against the *Staphylococcus aureus*, MRSA, *Escherichia coli*, *Pseudomonas aeruginosa*, and *Candida albicans*. Each dispersion was prepared at a concentration of 100 mg mL^{-1}, and 50 μL of each solution was placed into the wells. The method is explained in the ESI 3† in detail.[38–40]

2.2.8 Calculation of fractional inhibitory concentration index (FICI) to evaluate the synergistic activity of synthesized nanohybrids. The mean fractional inhibitory concentration index (FICI) was calculated to evaluate the potential synergistic interaction between nanohybrids, based on their previously reported minimum inhibitory concentrations (MICs). The FICI was determined using the following equation:[38]

$$\Sigma\text{FICI} = \text{FIC}_{(\text{nanohybrid A})} + \text{FIC}_{(\text{nanohybrid B})}$$

FIC = MIC of nanohybrid in combination/MIC of nanohybrid tested individually.

Based on the calculated FICI values, the interactions were classified as follows:

- ΣFICI < 1 indicates a synergistic effect,
- ΣFICI = 1 represents an additive effect, and
- ΣFICI > 1 suggests an antagonistic effect.

2.2.9 Determination of radical scavenging activity of metallic nanohybrids and their combinations with curcuminoids and turmeric oleoresins. Radical scavenging activity of monometallic, bimetallic, and trimetallic nanohybrids, as well as their combinations with curcuminoids and turmeric oleoresins, was evaluated using 2,2-diphenyl-1-picrylhydrazyl (DPPH) as a free radical. For the UV experiments, 0.1 mM DPPH solution was prepared by stirring the DPPH in methanol with a magnetic stirrer for 30 minutes. An equal amount of all 23 samples was dispersed in absolute methanol. Each of the test samples was mixed with an equal volume of the prepared DPPH solution and allowed to stand at room temperature for 30 minutes in the dark. After this incubation period, the absorbance of each solution was measured with a UV-vis spectrophotometer at a wavelength of 517 nm. The DPPH scavenging activity was calculated using the following formula:

$$\text{DPPH scavenging activity} = \frac{A_0 - A_1}{A_0} \times 100\%$$

where A_0 is the absorbance of the DPPH solution without the nanohybrid and A_1 is the absorbance of the DPPH solution with the nanohybrid at 517 nm.[41]

2.2.10 Statistical analysis. A statistical analysis was performed by analysis of variance (ANOVA) using MINITAB 18, and the significant difference of each sample was analyzed by Tukey and Fisher pairwise comparison at the significance level of 0.05.

2.2.11 Fabrication of metallic nanohybrids and curcuminoids incorporated electrospun nanofiber membranes. Four types of nanofiber membranes (A–D) were fabricated using electrospinning as: A – PCL-only membrane (PCL mat), B – PCL membrane loaded with 50% (w/w) trimetallic nanohybrid (T-PCL mat), C – PCL membrane loaded with 50% (w/w) curcuminoids (C-PCL mat), D – PCL membrane loaded with 25% (w/w) trimetallic nanohybrid + 25% (w/w) curcuminoids (T-C-PCL mat).

To fabricate the PCL mat, 240 mg of PCL was dissolved in 3 mL of acetone while continuously stirring for approximately 3 hours. The resulting solution was then transferred into a 10 mL syringe. The polymer blend was ejected from the syringe needle and deposited onto an aluminium foil collector. The electrospinning process was conducted using an SKE EF100 electrospinning system under ambient temperature and humidity, with the following parameters: a voltage of 16 kV, a tip-to-collector distance of 13 cm, and a flow rate of 1.5 mL h^{-1}.[42]

For the fabrication of all other mats, polymer blend solutions were prepared using 240 mg of respective materials. These solutions were sonicated for 4 to 5 hours at room temperature to ensure thorough dispersion of samples. After sonication, the

membranes were fabricated using the same electrospinning parameters.

2.2.12 Characterization of electrospun nanofiber mats. An X-ray diffraction (XRD) analysis was performed to investigate the crystal structure of metallic nanoparticles and curcuminoids within the membranes. Data were acquired using a Rigaku Ultima IV diffractometer equipped with a 3 kW sealed X-ray tube, operated at 40 kV and 30 mA. Membranes were scanned over a 2θ range of 20° to 80° at a scan rate of 1° min^{-1} with a 0.002° step width.

The nanofiber mats were analyzed using Raman spectroscopy with a Thermo Scientific DXR system, employing a red laser (λ = 785 nm) as the excitation source. Spectra were acquired over a range of 250 cm^{-1} to 2500 cm^{-1} using a fine laser power to prevent damage to the samples.

Surface morphological features of the electrospun membranes were observed using scanning electron microscopy (SEM) with a ZEISS model, utilizing the secondary electron method and an accelerated voltage of 10 kV. The average fiber diameter and its distribution for the membranes were calculated using ImageJ software (ImageJ 1.51).

Additionally, Energy dispersive X-ray spectrometry analysis (EDX) was performed along with the SEM, and EDX mapping was used to observe the distribution of relevant metal atoms throughout the sample.

2.2.13 Digestion of T-PCL mat and T-C-PCL mat to determine the composition of each metal in a unit area. The nanofiber mats were manually digested using a mixture of HCl and HNO_3 acids (3 : 1). For that 1 cm × 1 cm of five nanofiber mat pieces were taken from five different places of the mat and they were digested using 10 mL of acid mixture at 90 °C for 4 hours in a boiling tube. Then the digested samples were subjected to AAS analysis to determine the average composition of each metal in the respective mat.[43]

2.2.14 Release study of metal nanoparticles from T-PCL mat and T-C-PCL mat. A 3 cm × 3 cm section of the nanofiber mat was immersed in 10 mL of PBS medium at pH 5.5 for 24 hours. After this period, the solutions were analyzed using ICP-MS (Agilent Technologies model 7850) to determine whether metals were released from the PCL membranes.

2.2.15 Incorporated amounts and encapsulation efficiency of curcuminoids in C-PCL mat and T-C-PCL mat. To determine the total amount of curcuminoids effectively incorporated in nanofiber mats, a 1 cm × 1 cm piece of the respective mat was immersed in 2 mL of acetone, and the solution was stirred for 6 hours. Afterward, the absorbance of the filtrate was measured at a wavelength of 427 nm using a UV-vis spectrophotometer. The total amount of effectively incorporated curcuminoids was quantified using a previously established calibration curve. The encapsulation efficiency was calculated using the following equation.[44]

$$\text{Encapsulation efficiency} = \frac{W_A}{W_T} \times 100\%$$

where, W_A is the actual curcuminoids content, and W_T the is theoretical curcuminoids content in PCL electrospun nanofiber mats.

2.2.16 Release study of curcuminoids from T-C-PCL mat. The release study of curcuminoids from the T-C-PCL mat was determined by immersing a 3 cm × 3 cm piece of nanofiber mat in PBS (pH 5.5) medium. The released curcuminoids were quantified in 15 minutes, 30 minutes, 1-hour, 24-hours, 48-hour, and 72-hours intervals by UV-vis spectrophotometer at 427 nm wavelength.[45] To study the release mechanism, the experimental data of the release study were fitted into zeroth order, first order, Higuchi, and Korsmeyer-Peppas models. Since the solubility of curcuminoids is negligible in PBS, the sample was diluted with ethanol (1 : 1) when obtaining the absorbance values.

2.2.17 Determination of radical scavenging activity of electrospun nanofiber mats. Radical scavenging activity of nanofiber mats was evaluated using 2,2-diphenyl-1-picrylhydrazyl (DPPH) as a free radical. For the UV experiments, 0.1 mM DPPH solution was prepared by stirring the DPPH in methanol with a magnetic stirrer for 30 minutes. Two test tubes were filled with a 1 cm × 1 cm section of the respective fiber mat, 2 mL of distilled water, and 2 mL of prepared DPPH solution, and the resulting solutions were allowed to stand for 30 minutes in the dark. The absorbance of two solutions was measured with a UV-vis spectrophotometer at a wavelength of 517 nm. The DPPH scavenging activity was calculated using the following formula:

$$\text{DPPH scavenging activity} = \frac{A_0 - A_1}{A_0} \times 100\%$$

where A_0 is the absorbance of the DPPH solution without the sample and A_1 is the absorbance of the DPPH solution with the sample at 517 nm.[43]

2.2.18 Evaluation of the antimicrobial activity of the electrospun nanofiber mats. The disc diffusion method was carried out to investigate the antimicrobial activity of the metal NPs-curcuminoids based nanohybrids incorporated into nanofiber mats. PCL-mat, T-PCL mat, C-PCL mat, and T-C-PCL mat were tested against the ATCC cultures of Gram-positive bacteria; *Staphylococcus aureus* (ATCC 25923), methicillin-resistant *Staphylococcus aureus* (MRSA); Gram-negative bacteria; *Escherichia coli* (ATCC 25922), *Pseudomonas aeruginosa* (ATCC 27853), and fungi; *Candida albicans* (ATCC 10231). Erythromycin (15 μg) was used as the positive control for Gram-positive bacteria. Merepenem (15 μg) was used for *P. aeruginosa* and *E. coli*. Fluconazole (15 μg) was used as the positive control for fungi. A disc of PCL-mat was used as the negative control. The disposable micropipette tips as well as the media were autoclaved for 15 minutes at 121 °C and 15 bar of pressure. Other equipment made of glass was sterilized for two hours at 160 °C in a hot air furnace. Each expendable Petri plate was filled with 25 mL of agar medium (MHA for bacteria and SDA for fungi), which was then allowed to solidify. Once solidified, to obtain a confluent growth, a sterile cotton swab was first dipped into each microbial suspension and then gently streaked across the surface of the agar in a zigzag pattern, ensuring even distribution. The swab was then rotated to cover the entire plate, moving back and forth to spread the microorganisms. The previously described microbial strains were used to produce microbial

suspensions. Then the prepared discs were placed on the agar surface by using sterile forceps. Each plate was incubated at 37 °C for 24 hours. Next, using a Netillin Zone Reader (USA), the zone of inhibition over every disc was calculated. Every technique was carried out in triplicate in compliance with CLSI recommendations, M27 guidelines for *C. albicans*.[43]

The mean value of the zones of inhibition of each nanofiber mat against all the chosen microbial strain was statistically analyzed using a Tukey pairwise comparison test at the significance level of 0.05.

3 Results and discussion

The integration of metal nanoparticles, turmeric oleoresin, and curcuminoids into electrospun polymeric films represents a groundbreaking solution for developing highly effective antimicrobial materials. This research focuses on creating these innovative electrospun films that combine metal nanoparticles with turmeric oleoresin and curcuminoids, paving the way for safer and more efficient health applications. By harnessing the synergistic antibacterial properties of various metal nanoparticles in conjunction with curcuminoids, this approach offers a significant leap forward compared to relying solely on individual nanoparticles. The combination of metals with curcuminoids not only enhances antibacterial efficacy but also through a synergistic mechanism that is far more powerful than the effects of any single metal alone.[46]

In our study, we specifically chose three metals—silver (Ag), copper (Cu), and nickel (Ni)—that are renowned for their ability to disrupt microbial cell membranes, inhibit protein synthesis, and induce oxidative stress. These mechanisms collectively enable them to combat a broad spectrum of bacterial pathogens effectively. The synthesized nanohybrids, along with the curcuminoids, were thoroughly evaluated through structural and morphological characterization, as well as rigorous antibacterial assays, revealing their potential as next-generation antimicrobial agents.

Curcuminoids, the powerful active compounds derived from turmeric, are widely acknowledged for their potent antioxidant and anti-inflammatory properties. Their antioxidant capabilities allow curcuminoids to effectively neutralize free radicals and diminish oxidative stress, which are significant contributors to a range of diseases and the aging process. Moreover, curcuminoids excel at modulating inflammatory responses, showcasing remarkable therapeutic potential for numerous inflammation-related conditions. The generation of reactive oxygen species (ROS) by silver (Ag), copper (Cu), and nickel (Ni) nanoparticles is pivotal in their antimicrobial effectiveness as they induce oxidative stress and inflict damage on microbial cells. By combining these metal nanoparticles with curcuminoids, we significantly enhance both the antioxidant and antimicrobial properties of the formulation. Curcuminoids not only scavenge ROS, mitigating the risks associated with excess oxidative stress, but also amplify the antimicrobial activity of the metal nanoparticles. In our study, we performed a DPPH assay to gauge radical scavenging activity along with antimicrobial activity, to assess the antioxidant effects of the metal nanoparticles alone and in conjunction with curcuminoids and oleoresin. Our findings clearly demonstrated that the combination of the multimetallic nanohybrid and curcuminoids achieved the highest radical scavenging activity and exhibited remarkable antimicrobial effects compared to other nanohybrids. This compelling evidence highlights the synergistic effects responsible for the enhanced activity of multimetallic nanohybrids when paired with curcuminoids, making a strong case for their application in health and wellness solutions.

3.1 Identification of oleoresin and curcuminoids crystals by thin layer chromatography (TLC)

The moisture content of dried turmeric slices was 9.35%, as this level is suitable for extraction processes, it was concluded that the turmeric powder was adequately dried.

Curcuminoids, which are found in the rhizome of turmeric, consist of curcumin, demethoxycurcumin (DMC), and bisdemethoxycurcumin (BDMC) prior to recrystallization, the extracted turmeric oleoresin was analyzed using thin-layer chromatography (TLC). Fig. S2† presents the TLC for turmeric oleoresin (TOR) and curcuminoids crystals (CC).

It clearly demonstrates that the extracted turmeric oleoresin contains curcumin, DMC, and BDMC, as shown by the matching bands and similar Rf values to the reference standards. The clear separation of the bands indicates a good resolution, suggesting that the TLC conditions are suitable for analyzing curcuminoids. The slight differences in Rf for DMC and BDMC may be attributed to variation in the chemical environments of the reference and extracted samples. According to the TLC results of the purified curcuminoids crystals, which closely match the reference standards in Rf values and band patterns, confirming the reliability of the purification process. Table 2(a) and (b) display the calculated Rf values for the turmeric oleoresin and curcuminoids crystals, in comparison to the standard curcuminoids. Similar results have been reported by previous work,[47] which are closely matched with Rf values of curcumin, DMC,

Table 2 (a) Rf values for turmeric oleoresin (TOR) and reference curcuminoids (Ref). (b) Rf values for curcuminoids crystals (CC) and reference curcuminoids (Ref)[a]

Compound	Rf values for ref	Rf values for TOR
(a)		
Curcumin	0.804	0.804
DMC	0.674	0.717
BDMC	0.500	0.565
Compound	**Rf values for ref**	**Rf values for CC**
(b)		
Curcumin	0.738	0.738
DMC	0.476	0.500
BDMC	0.333	0.333

[a] The quantification and characterization of oleoresin and curcuminoids have explained in ESI 4, in detail.[48–50]

and BDMC. Furthermore, curcumin, considered as the major component in natural turmeric, has the highest intensity spot.

3.2 Evaluation of anti-inflammatory activity of curcuminoids

The anti-inflammatory activity of the various curcuminoid formulations was evaluated using the egg albumin assay, a well-established model for assessing inflammation. The results (Fig. S3(c)†) demonstrated that the highest concentrations of curcuminoids exhibited the strongest anti-inflammatory effects, while the lower concentrations showed reduced activity. This dose-dependent response is consistent with the known pharmacokinetics and biological activity of curcuminoids, where higher concentrations typically lead to more pronounced effects on inflammation. At elevated concentrations, curcuminoids are more likely to bind to key inflammatory mediators, such as pro-inflammatory enzymes and cytokines, thereby inhibiting the pathways involved in inflammation.

Curcuminoids, particularly curcumin, have been widely recognized for their ability to modulate inflammatory pathways, primarily by inhibiting cyclooxygenase (COX) and lipoxygenase (LOX), which are enzymes involved in the production of inflammatory mediators like prostaglandins and leukotrienes.[32] In the higher concentrations used in this assay, the curcuminoids may be present in sufficient quantities to effectively interfere with these enzymes and the release of pro-inflammatory cytokines, thus reducing the inflammatory response more substantially. The reduced anti-inflammatory activity at lower concentrations suggests that a threshold concentration must be reached for curcuminoids to exert a significant impact, which is a common characteristic of compounds that act through enzyme inhibition or receptor binding.

The anti-inflammatory results also highlight the importance of concentration in curcuminoid formulations. As demonstrated in this study, the effectiveness of curcuminoids is dose-dependent, suggesting that careful consideration of concentration is critical for maximizing their anti-inflammatory potential in both pharmaceutical and biomedical applications. These findings not only validate the potential of curcuminoids as anti-inflammatory agents but also emphasize the importance of incorporating them into multifunctional formulations, such as the metal nanoparticle-curcuminoid nanohybrids developed in this study, which can offer synergistic effects for enhanced therapeutic outcomes.

3.3 Characterization of synthesized Ag, Cu, and Ni nanohybrids

ESI 5 and Fig. S4† show the detailed characterizations PXRD, FTIR, Raman, optical band gap, SEM, and particle size distribution of synthesized Ag, Cu, and Ni nanoparticles.[51–56] Fig. S5† shows the EDX mapping of synthesized Ag, Cu, and Ni nanoparticles.

3.4 Particle size analysis and zeta potential for trimetallic nanoparticle combination

The interactions between various nanoparticle types in a mixed nanoparticle system might affect the zeta potential. Every kind of nanoparticle may have a different surface charge, and ion exchange and electrostatic interactions may cause their zeta potentials to alter when combined. Since it was taken into consideration for the electrospinning process, the zeta potential of the mixed nanoparticle system was measured in this investigation. In this study, the average zeta potential for the Ag, Cu, and Ni nanoparticle system is -25.37 ± 4.39 mV in water (Fig. S6†). While similarly charged nanoparticles may repel one another in a mixed solution, oppositely charged ones may attract and cause aggregation. High ionic strength can also encourage aggregation and lessen repulsion.[57] The particles are considered to have moderate stability if the zeta potential is between -30 and +30 mV, which means that aggregation may still be a possibility.[58]

Fig. S7† depicts the particle size distribution of the Ag, Cu, and Ni nanoparticle system, and the average particle size is 714.5 nm. This higher value may indicate some aggregations in the sample.

A large negative zeta potential prevents metallic nanoparticles from aggregating; however, certain conditions can overcome this repulsion. When electrostatic screening lowers repulsion in high-ionic strength solutions, van der Waals forces prevail and produce agglomeration.[59]

Additionally, research on electrostatic forces and the electrical double layer shows how ions in solution affect particle interactions and stability. The electrical double layer collapses at high ionic strength, reducing repulsion and increasing aggregation.[60]

3.5 Evaluation of MIC, MBC, and IC_{50} of metallic nanohybrids and their combinations with curcuminoids and turmeric oleoresin

Metal nanoparticles have generated significant attention in recent years due to their unique antimicrobial properties. These stem from their small size, high surface area, and ability to interact with microbial cells in ways that bulk materials cannot. When metal nanoparticles are combined with bioactive compounds such as curcuminoids, their antimicrobial activity can be further enhanced.

In this study, antimicrobial testing revealed that the trimetallic nanohybrid combined with curcuminoids exhibited the lowest values for minimum inhibitory concentration (MIC), minimum bactericidal concentration (MBC), minimum fungicidal concentration (MFC), and half-maximal inhibitory concentration (IC_{50}) across all tested microorganisms. This indicates a significant synergistic effect of the trimetallic nanohybrid and curcuminoids formulation compared to the monometallic and bimetallic nanohybrids and their combinations with curcuminoids. Specifically, the trimetallic nanohybrid demonstrated enhanced antimicrobial efficacy when compared to both the bimetallic and monometallic nanohybrids, as evidenced by lower MIC values that indicate a greater inhibition of microbial growth at lower concentrations. The MIC, MBC, and MFC results further supported this observation, showing that the trimetallic nanohybrid combined with curcuminoids required the lowest concentration to achieve

Table 3 The MIC, MBC and the IC_{50} values of respective nanohybrid samples against test organisms

Type of the nanohybrid	*S. aureus* (mg mL^{-1})			MRSA (mg mL^{-1})			*E. coli* (mg mL^{-1})			*P. aeruginosa* (mg mL^{-1})			*C. albicans* (mg mL^{-1})		
	MIC	MBC	IC_{50}	MIC	MBC	IC_{50}	MIC	MBC	IC_{50}	MIC	MBC	IC_{50}	MIC	MFC	IC_{50}
Ag	0.156 ± 0.00	0.156 ± 0.00	0.2985	0.156 ± 0.00	0.312 ± 0.00	0.3117	0.156 ± 0.00	0.312 ± 0.00	0.3418	0.312 ± 0.00	0.625 ± 0.00	0.4461	0.156 ± 0.00	0.312 ± 0.00	0.2872
Cu	0.156 ± 0.00	0.312 ± 0.00	0.4499	0.312 ± 0.00	0.625 ± 0.00	0.5382	0.156 ± 0.00	0.312 ± 0.00	0.3621	0.312 ± 0.00	0.625 ± 0.00	0.546	0.312 ± 0.00	0.625 ± 0.00	0.3621
Ni	0.625 ± 0.00	1.250 ± 0.00	0.8682	0.625 ± 0.00	1.250 ± 0.00	0.9252	0.625 ± 0.00	1.250 ± 0.00	1.186	1.250 ± 0.00	2.50 ± 0.00	1.114	0.625 ± 0.00	1.250 ± 0.00	0.8682
Ag + Cu	0.078 ± 0.00	0.156 ± 0.00	0.1831	0.078 ± 0.00	0.156 ± 0.00	0.1948	0.156 ± 0.00	0.312 ± 0.00	0.2517	0.156 ± 0.00	0.312 ± 0.00	0.2876	0.156 ± 0.00	0.312 ± 0.00	0.1831
Ag + Ni	0.625 ± 0.00	1.250 ± 0.00	0.2902	0.625 ± 0.00	1.250 ± 0.00	0.2892	0.312 ± 0.00	0.625 ± 0.00	0.4175	0.625 ± 0.00	1.250 ± 0.00	0.2501	0.312 ± 0.00	0.625 ± 0.00	0.2902
Cu + Ni	1.250 ± 0.00	2.50 ± 0.00	0.5356	1.250 ± 0.00	2.50 ± 0.00	0.3654	0.625 ± 0.00	1.250 ± 0.00	0.5137	1.250 ± 0.00	2.50 ± 0.00	0.3389	0.625 ± 0.00	1.250 ± 0.00	0.5137
Ag + Cu + Ni	0.078 ± 0.00	0.078 ± 0.00	0.185	0.078 ± 0.00	0.156 ± 0.00	0.1941	0.078 ± 0.00	0.156 ± 0.00	0.1826	0.156 ± 0.00	0.312 ± 0.00	0.2606	0.078 ± 0.00	0.156 ± 0.00	0.1824
Curcuminoids	0.078 ± 0.00	0.156 ± 0.00	0.3106	0.078 ± 0.00	0.156 ± 0.00	0.3452	0.078 ± 0.00	0.156 ± 0.00	0.3751	0.156 ± 0.00	0.312 ± 0.00	0.4712	0.078 ± 0.00	0.156 ± 0.00	0.2955
Ag + curcuminoids	0.078 ± 0.00	0.156 ± 0.00	0.2062	0.078 ± 0.00	0.156 ± 0.00	0.1608	0.156 ± 0.00	0.312 ± 0.00	0.1753	0.312 ± 0.00	0.625 ± 0.00	0.2244	0.078 ± 0.00	0.156 ± 0.00	0.1459
Cu + curcuminoids	0.156 ± 0.00	0.312 ± 0.00	0.2263	0.078 ± 0.00	0.156 ± 0.00	0.2725	0.156 ± 0.00	0.312 ± 0.00	0.1867	0.156 ± 0.00	0.312 ± 0.00	0.2735	0.156 ± 0.00	0.312 ± 0.00	0.1867
Ni + curcuminoids	0.625 ± 0.00	1.250 ± 0.00	0.4401	0.312 ± 0.00	0.625 ± 0.00	0.4667	0.625 ± 0.00	0.125 ± 0.00	0.5947	1.250 ± 0.00	2.50 ± 0.00	0.5594	0.156 ± 0.00	0.312. ± 0.00	0.4401
Ag + Cu + curcuminoids	0.078 ± 0.00	0.156 ± 0.00	0.09189	0.078 ± 0.00	0.156 ± 0.00	0.09887	0.156 ± 0.00	0.312 ± 0.00	0.127	0.078 ± 0.00	1.560 ± 0.00	0.1464	0.078 ± 0.00	0.156 ± 0.00	0.09189
Ag + Ni + curcuminoids	0.312 ± 0.00	0.625 ± 0.00	0.1478	0.312 ± 0.00	0.625 ± 0.00	0.147	0.312 ± 0.00	0.625 ± 0.00	0.21	0.625 ± 0.00	1.250 ± 0.00	0.129	0.156 ± 0.00	0.312 ± 0.00	0.1478
Cu + Ni + curcuminoids	1.250 ± 0.00	2.50 ± 0.00	0.2712	1.250 ± 0.00	2.50 ± 0.00	0.1863	1.250 ± 0.00	2.50 ± 0.00	0.2571	1.250 ± 0.00	2.50 ± 0.00	0.1708	0.312 ± 0.00	0.625 ± 0.00	0.2571
Ag + Cu + Ni curcuminoids	0.039 ± 0.00	0.078 ± 0.00	0.09274	0.039 ± 0.00	0.078 ± 0.00	0.09725	0.039 ± 0.00	0.078 ± 0.00	0.09195	0.078 ± 0.00	0.156 ± 0.00	0.1322	0.039 ± 0.00	0.078 ± 0.00	0.09218
Oleoresin	0.312 ± 0.00	0.625 ± 0.00	0.4012	0.312 ± 0.00	0.625 ± 0.00	0.4125	0.312 ± 0.00	0.625 ± 0.00	0.4519	0.625 ± 0.00	1.250 ± 0.00	0.5122	0.312 ± 0.00	0.625 ± 0.00	0.3546
Ag + oleoresin	0.156 ± 0.00	0.312 ± 0.00	0.2204	0.156 ± 0.00	0.312 ± 0.00	0.2288	0.156 ± 0.00	0.312 ± 0.00	0.2451	0.312 ± 0.00	0.625 ± 0.00	0.3127	0.156 ± 0.00	0.312 ± 0.00	0.2093
Cu + oleoresin	0.312 ± 0.00	0.625 ± 0.00	0.3147	0.312 ± 0.00	0.625 ± 0.00	0.38	0.312 ± 0.00	0.625 ± 0.00	0.2584	0.625 ± 0.00	1.250 ± 0.00	0.383	0.312 ± 0.00	0.625 ± 0.00	0.2584
Ni + oleoresin	0.625 ± 0.00	1.250 ± 0.00	0.6072	0.625 ± 0.00	1.250 ± 0.00	6491	0.625 ± 0.00	0.125 ± 0.00	0.8441	1.250 ± 0.00	2.50 ± 0.00	0.8003	0.312 ± 0.00	0.625 ± 0.00	0.6072
Ag + Cu + oleoresin	0.078 ± 0.00	0.156 ± 0.00	0.1316	0.078 ± 0.00	0.156 ± 0.00	0.2204	0.156 ± 0.00	0.312 ± 0.00	0.1755	0.078 ± 0.00	1.560 ± 0.00	0.2045	0.078 ± 0.00	0.156 ± 0.00	0.1316
Ag + Ni + oleoresin	0.625 ± 0.00	1.250 ± 0.00	0.2064	0.312 ± 0.00	0.625 ± 0.00	0.3147	0.625 ± 0.00	1.250 ± 0.00	0.2895	0.625 ± 0.00	1.250 ± 0.00	0.1754	0.312 ± 0.00	0.625 ± 0.00	0.2064
Cu + Ni + oleoresin	1.250 ± 0.00	2.50 ± 0.00	0.3782	1.250 ± 0.00	2.50 ± 0.00	0.6072	1.250 ± 0.00	2.50 ± 0.00	0.3617	2.50 ± 0.00	5.00 ± 0.00	0.2455	0.312 ± 0.00	0.625 ± 0.00	0.3617
Ag + Cu + Ni + oleoresin	0.078 ± 0.00	0.156 ± 0.00	0.1323	0.078 ± 0.00	0.156 ± 0.00	0.1382	0.078 ± 0.00	0.156 ± 0.00	0.1313	0.156 ± 0.00	0.312 ± 0.00	0.1821	0.156 ± 0.00	0.312 ± 0.00	0.1313

complete microbial kill, as indicated by the resazurin dye remaining blue.

Additionally, the IC_{50} values confirmed that the trimetallic nanohybrid and curcuminoids were more effective at inhibiting microbial growth compared to their monometallic and bimetallic counterparts and their combinations with curcuminoids. Notably, the turmeric oleoresin yielded higher MIC and MBC values compared to curcuminoids against all tested microbial strains, which may be attributed to the lower purity level of the turmeric oleoresin. These findings emphasize the enhanced synergistic activity of the trimetallic nanohybrids in combination with curcuminoids, highlighting their superior potential for applications in areas such as wound dressings, where effective antimicrobial properties are critical. Table 3 presents the MIC, MBC, and IC_{50} values of the respective test samples. IC_{50} graphs were constructed for each nanohybrid by performing curve fitting with a nonlinear regression model using the software GraphPad Prism. Fig. S8† presents the IC_{50} graphs for each nanohybrid.[43]

3.6 Evaluation of the synergistic activity of synthesized nanohybrids using fractional inhibitory concentration index (FICI)

The synergistic activity of the synthesized nanohybrids was further confirmed by calculating the FIC index. Table S1† depicts the FICI for curcuminoids and oleoresin. The results clearly indicate that the most effective nanohybrid combination is the trimetallic formulation with curcuminoids (Ag + Cu + Ni + curcuminoids), which consistently exhibits either synergistic or additive antimicrobial activity against all tested pathogens (*S. aureus*, MRSA, *E. coli*, *P. aeruginosa*, *and C. albicans*). Unlike the other combinations, which display variable effects, fluctuating between antagonistic, additive, or occasionally synergistic responses depending on the pathogen, the trimetallic–curcuminoid hybrid maintains a reliable therapeutic profile with no antagonistic interactions observed. This suggests a favorable cooperative effect among the three metals and curcuminoids, enhancing broad-spectrum antimicrobial efficacy and making this hybrid the most promising candidate for further development.

3.7 Evaluation of well-diffusion assay of metallic nanoparticles and their combinations with curcuminoids and turmeric oleoresins

Fig. S9† shows the images of the respective inhibition zones of each nanohybrid, and Table 4 shows the values of inhibition zones.

The well diffusion assay was conducted to evaluate the antimicrobial efficacy of 23 different samples, including individual metal nanoparticles (Ag, Cu, Ni), combinations of metals (Ag + Cu, Ag + Ni, Cu + Ni, Ag + Cu + Ni), metal nanoparticles combined with curcuminoids (CS) and turmeric oleoresin

Table 4 The values of inhibition zones[a]

	Inhibition zone (mm)			
Type of the nanohybrid	*S. aureus*	*E. coli*	*P. aeruginosa*	*C. albicans*
Positive control	25.50 ± 0.41^{a}	26.00 ± 1.00^{a}	28.33 ± 0.47^{a}	31.50 ± 0.41^{a}
Negative control	00.00 ± 0.00^{b}	00.00 ± 0.00^{b}	00.00 ± 0.00^{b}	00.00 ± 0.00^{b}
Ag	14.33 ± 0.47^{c}	15.67 ± 0.58^{cj}	13.33 ± 1.00^{cd}	15.33 ± 0.47^{cdk}
Cu	12.67 ± 0.58^{d}	13.33 ± 0.47^{d}	12.00 ± 1.00^{dg}	14.00 ± 1.00^{d}
Ni	8.50 ± 0.41^{e}	9.67 ± 0.58^{e}	9.00 ± 1.00^{e}	10.50 ± 0.41^{ef}
Ag + Cu	16.50 ± 0.41^{f}	16.50 ± 0.41^{ch}	14.33 ± 0.47^{fk}	15.67 ± 0.24^{chk}
Ag + Ni	12.37 ± 0.24^{d}	13.33 ± 0.47^{d}	11.67 ± 0.24^{g}	14.50 ± 0.41^{dk}
Cu + Ni	9.33 ± 0.47^{el}	10.50 ± 0.41^{el}	9.33 ± 0.47^{e}	10.00 ± 0.00^{f}
Ag + Cu + Ni	18.67 ± 0.24^{g}	19.33 ± 0.47^{f}	17.67 ± 0.24^{hi}	20.00 ± 1.00^{g}
Curcuminoids (CS)	10.50 ± 0.41^{h}	11.00 ± 1.00^{gl}	9.67 ± 0.24^{e}	10.00 ± 0.00^{f}
Ag + CS	15.33 ± 0.47^{i}	15.67 ± 0.24^{cj}	13.67 ± 0.24^{ck}	16.00 ± 1.00^{ch}
Cu + CS	12.67 ± 0.24^{d}	14.00 ± 1.00^{d}	12.00 ± 1.00^{dg}	15.67 ± 0.24^{chk}
Ni + CS	9.33 ± 0.47^{el}	9.67 ± 0.24^{e}	9.33 ± 0.47^{e}	10.67 ± 0.24^{ef}
Ag + Cu + CS	17.67 ± 0.24^{j}	19.33 ± 0.47^{f}	16.67 ± 0.24^{i}	16.67 ± 0.24^{h}
Ag + Ni + CS	14.33 ± 0.47^{c}	16.67 ± 0.24^{h}	14.33 ± 0.47^{fk}	15.67 ± 0.24^{chk}
Cu + Ni + CS	10.33 ± 0.47^{h}	11.50 ± 0.41^{g}	10.00 ± 0.00^{e}	11.67 ± 0.24^{e}
Ag + Cu + Ni + CS	20.33 ± 0.47^{k}	21.50 ± 0.41^{i}	19.00 ± 1.00^{j}	24.67 ± 0.24^{i}
Turmeric oleoresin (TOR)	9.33 ± 0.47^{el}	9.67 ± 0.24^{e}	9.00 ± 1.00^{e}	10.00 ± 0.00^{f}
Ag + TOR	14.67 ± 0.24^{ci}	15.33 ± 0.47^{j}	13.33 ± 0.47^{ck}	15.67 ± 0.24^{chk}
Cu + TOR	12.67 ± 0.24^{d}	13.33 ± 0.47^{d}	12.00 ± 1.00^{dg}	15.00 ± 1.00^{cdk}
Ni + TOR	9.00 ± 0.50^{e}	9.67 ± 0.24^{e}	9.00 ± 1.00^{e}	10.00 ± 0.00^{f}
Ag + Cu + TOR	16.33 ± 0.47^{f}	18.33 ± 0.47^{k}	15.00 ± 1.00^{f}	16.00 ± 1.00^{ch}
Ag + Ni + TOR	15.33 ± 0.47^{i}	15.67 ± 0.24^{cj}	13.00 ± 1.00^{cd}	15.33 ± 0.47^{cdk}
Cu + Ni + TOR	10.00 ± 0.00^{hl}	11.00 ± 1.00^{gl}	10.00 ± 0.00^{e}	11.33 ± 0.47^{ef}
Ag + Cu + Ni + TOR	19.33 ± 0.47^{g}	20.67 ± 0.24^{i}	18.00 ± 1.00^{hj}	22.67 ± 0.24^{j}

[a] Values followed by different superscripts in the same column are significantly different ($P < 0.05$) according to Fisher pairwise comparison test ($n = 3$).

(TOR), and other control formulations. Among these samples, the highest inhibition zone was observed in the combination of Ag + Cu + Ni + CS, which exhibited superior antimicrobial activity against all the tested microbial strains. This enhanced efficacy can be attributed to the synergistic interaction between the metal nanoparticles and curcuminoids. The individual metal nanoparticles (Ag, Cu, Ni) exert antimicrobial activity *via* distinct mechanisms, such as the release of metal ions that interfere with bacterial cell walls and DNA replication. When combined, the metals likely interact in a way that amplifies these effects, leading to a broader and more potent antimicrobial response. Additionally, curcuminoids, known for their anti-inflammatory and antimicrobial properties, can further enhance this activity by disrupting microbial cell membranes and inhibiting vital enzymes. The result is a compounded antimicrobial effect that surpasses that of any single component.

Interestingly, the inhibition zones observed for turmeric oleoresin (TOR) were lower than those for the curcumin standard (CS). This discrepancy can be explained by the difference

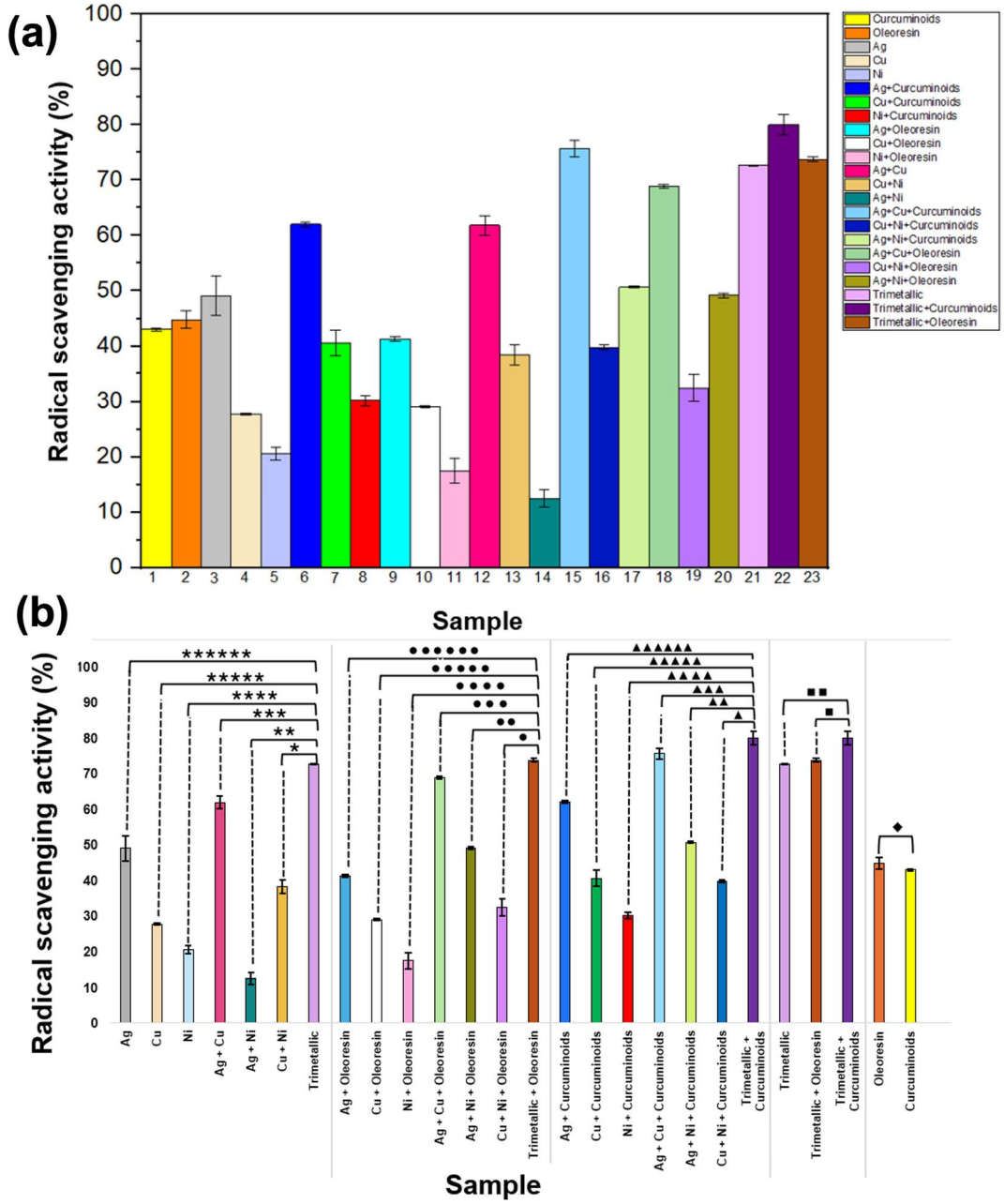

Fig. 2 (a) Radical scavenging activity of fabricated metal nanohybrids, turmeric oleoresin, curcuminoids, and their combinations. (b) The % radical scavenging activities of different samples. (b) The significant difference between (******) Ag, (*****) Cu, (****) Ni, (***) Ag + Cu, (**) Ag + Ni, (*) Cu + Ni with trimetallic nanohybrid, (●●●●●●) Ag + OR, (●●●●●) Cu + OR, (●●●●) Ni + OR, (●●●) Ag + Cu + OR, (●●) Ag + Ni + OR, (●) Cu + Ni + OR with trimetallic + OR, (▲▲▲▲▲▲) Ag + CS, (▲▲▲▲▲) Cu + CS, (■) trimetallic + OR with trimetallic + CS, and (◆) OR with CS.

in purity levels. Curcuminoids in the form of CS represent a more concentrated and purified active compound, whereas TOR contains a mixture of compounds with varying degrees of bioactivity. As a result, curcuminoids exhibit a stronger antimicrobial effect compared to turmeric oleoresin, which has a lower concentration of active curcuminoid compounds.

The combination of metal nanoparticles and curcuminoids offers several distinct advantages over using the individual agents alone. First, the use of metal nanoparticles in combination with curcuminoids enhances the antimicrobial potency through a synergistic effect. The metals contribute to a broad-spectrum antimicrobial activity, while the curcuminoids not only provide additional antimicrobial action but also offer well-documented anti-inflammatory and antioxidant properties, which help mitigate inflammation and support tissue healing. Moreover, the inclusion of curcuminoids, which are naturally derived from turmeric, offers an added benefit of reducing the overall toxicity of the system. Curcuminoids have long been recognized for their therapeutic potential in traditional medicine, being non-toxic at appropriate doses and offering a natural alternative to synthetic antimicrobial agents. The inclusion of these bioactive compounds helps to balance the overall toxicity of the formulation, ensuring a safer and more sustainable approach compared to using solely metallic agents that may pose environmental or health risks.

Additionally, the combination of these agents enhances the material's effectiveness against microbial resistance. As resistance to single antimicrobial agents becomes an increasing challenge, the use of a multi-faceted approach involving metal nanoparticles and curcuminoids can help overcome this barrier. The combination also offers a broader spectrum of action, addressing a wide variety of pathogens, including resistant strains that might not be affected by conventional antibiotics.

3.8 DPPH assay for evaluating the radical scavenging activity of metal nanohybrids, turmeric oleoresin, curcuminoids, and their combinations

As depicted in Fig. 2a, the metal nanohybrids can be categorized into three groups: monometallic (3–11), bimetallic (12–20), and trimetallic (21–23). Metal nanoparticles exhibit radical scavenging activity by generating reactive oxygen species (ROS), while curcuminoids and oleoresin exhibit radical scavenging activity due to their antioxidant qualities. Among monometallic nanoparticles -Ag, Cu, and Ni (3, 4, and 5)-Ag demonstrates the highest level of radical scavenging activity, with the others showing varying degrees. The combination of these monometallic nanoparticles with curcuminoids generally enhances their radical scavenging activity due to a synergistic effect. For example, the pairing of Ag with curcuminoids (6) and Cu with curcuminoids (7) results in significantly improved radical scavenging activity compared to the individual metals, indicating that the presence of curcuminoids amplifies the activity. Additionally, two bimetallic combinations of Ag, Cu, and Ni (12 and 13) exhibit a notable increase in radical scavenging activity compared to their monometallic counterparts.

This enhancement can be attributed to the synergistic interactions between different metals. The inclusion of curcuminoids or oleoresin further enhanced the radical scavenging activity of these bimetallic nanohybrids. Ag + Cu + curcuminoids (15) and Ag + Cu + oleoresin (18) exhibited strong radical scavenging activity, indicating a potent combined antioxidant effect. The trimetallic nanohybrids, both on their own (21) and in conjunction with curcuminoids (22) or oleoresin (23), exhibited the highest radical scavenging activity. This suggests a synergistic effect where multiple metals interact with bioactive compounds to achieve optimal radical scavenging.[61] Among them, the trimetallic nanohybrid combined with curcuminoids exhibited the highest activity in this study, highlighting the significance of interactions between multiple metals and natural antioxidants. There was no significant difference in radical scavenging activity between curcuminoids (1) and oleoresin (2). These findings further confirm the enhanced synergistic activity of the trimetallic nanohybrids when combined with curcuminoids, making them suitable for applications that require effective antimicrobial properties. Table 5 shows the percentage of radical scavenging activity of various combinations of nanohybrids, curcuminoids, and oleoresin.

A statistical analysis was performed to identify that there is a significant difference between the mean value of % radical scavenging activities of all 23 samples. Fig. 2b shows the comparison of the % radical scavenging activities of those different samples.

Table 5 The percentage radical scavenging activity of various combinations of nanohybrids, curcuminoids and oleoresin[a]

Nanohybrid type	Radical scavenging activity (%)
Curcuminoids	43.04 ± 0.23^{ae}
Oleoresin	44.78 ± 1.61^{aei}
Ag	49.11 ± 3.57^{ai}
Cu	27.78 ± 0.18^{bc}
Ni	20.66 ± 1.17^{cf}
Ag + curcuminoids	61.98 ± 0.41^{d}
Cu + curcuminoids	40.63 ± 2.32^{e}
Ni + curcuminoids	30.17 ± 0.86^{b}
Ag + oleoresin	41.28 ± 0.45^{e}
Cu + oleoresin	29.09 ± 0.19^{b}
Ni + oleoresin	17.47 ± 2.25^{fg}
Ag + Cu	61.83 ± 1.74^{d}
Cu + Ni	38.41 ± 1.90^{ek}
Ag + Ni	12.50 ± 1.57^{g}
Ag + Cu + curcuminoids	75.65 ± 1.49^{hj}
Cu + Ni + curcuminoids	39.81 ± 0.40^{e}
Ag + Ni + curcuminoids	50.72 ± 0.21^{i}
Ag + Cu + oleoresin	68.91 ± 0.29^{dh}
Cu + Ni + oleoresin	32.51 ± 2.35^{bk}
Ag + Ni + oleoresin	49.20 ± 0.41^{ai}
Trimetallic	72.65 ± 0.06^{h}
Trimetallic + curcuminoids	80.04 ± 1.88^{j}
Trimetallic + oleoresin	73.78 ± 0.42^{hj}

[a] Values followed by different superscripts in the same column are significantly different ($P < 0.05$) according to Tukey's pairwise comparison test ($n = 3$).

All the samples of metals have lower p values than the significance level of 0.05. So, it can be interpreted that there is a significant difference between the mean values of radical scavenging activity of monometallic nanohybrids and trimetallic nanohybrids, bimetallic nanohybrids and trimetallic nanohybrids, at the significance level of 0.05, when equal variance is assumed.

There is a significant difference between the mean values of radical scavenging activity of monometallic nanohybrids + curcuminoids and trimetallic nanohybrids + curcuminoids, bimetallic nanohybrids + curcuminoids and trimetallic nanohybrids + curcuminoids, at the significance level of 0.05, when equal variance is assumed. However, there is one exception, the significant difference between the bimetallic nanohybrid, Ag + Cu + curcuminoids and the trimetallic nanohybrid; Ag + Cu + Ni + curcuminoids showed no difference. This result reveals there is no significant difference between these radical scavenging activities, however, when analyzing the antimicrobial data, it can be clearly understood that the trimetallic nanohybrid of Ag + Cu + Ni curcuminoids is superior over the bimetallic nanohybrid of Ag + Cu + curcuminoids. Therefore, when considering both radical scavenging activity and the antimicrobial activity, it can be concluded that using the trimetallic nanohybrid of Ag + Cu + Ni curcuminoids is advantageous over the bimetallic nanohybrid of Ag + Cu + curcuminoids.

The mean values of radical scavenging activity of trimetallic and trimetallic + curcuminoids, have lower p values than the significance level of 0.05. So, it can be interpreted that there is a significant difference between the mean values of radical scavenging activity at the significance level of 0.05, when equal variance is assumed.

The reported p value for oleoresin and curcuminoids is higher than 0.05. Hence, it can be interpreted that there is no

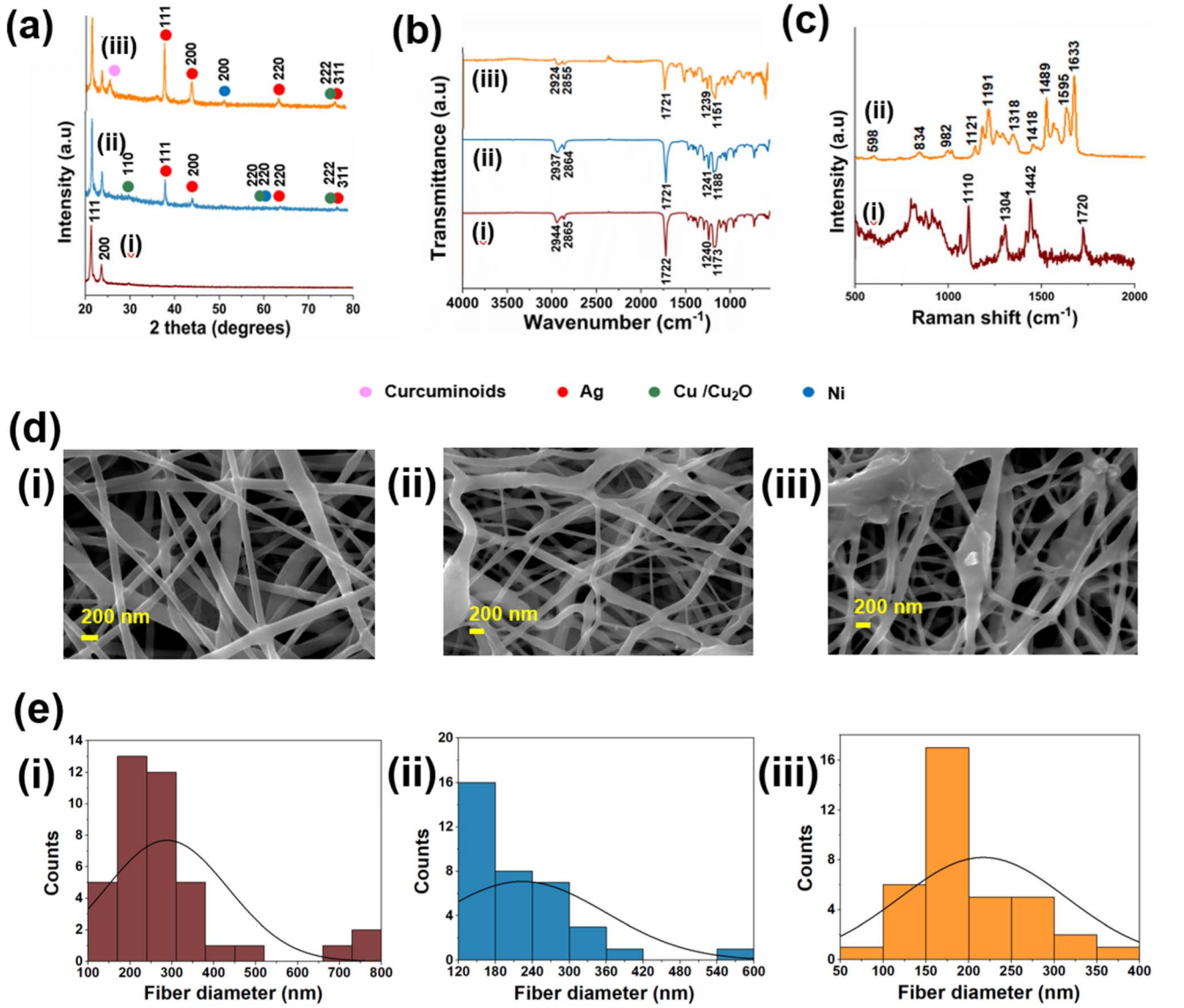

Fig. 3 (a) PXRD pattern (b) FTIR spectrum of (i) PCL mat, (ii) T-PCL mat (iii) T-C-PCL mat (c) Raman spectrum of (i) PCL mat, (ii) T-C-PCL mat (d) SEM images (e) fiber diameter distribution of (i) PCL mat, (ii) T-PCL mat, and (iii)T-C-PCL mat.

significant difference between oleoresin and curcuminoids, and the significance level of 0.05, when equal variance is assumed.

3.9 Characterization of fabricated electrospun membranes

The electrospun nanofiber mats were initially analyzed using XRD to confirm the successful incorporation of trimetallic nanohybrid and its combination with curcuminoids into the PCL membrane. Fig. 3a illustrates the XRD pattern of PCL mat, the T-PCL mat, and T-C-PCL mat. According to Fig. 3a(i), the XRD pattern for the PCL membrane reveals two characteristic peaks at 21.3° and 24° (2θ values), corresponding to the (110) and (200) crystallographic planes, indicative of the semi-crystalline nature of PCL polymer.[62] Fig. 3a(ii) depicts the XRD pattern for the T-PCL mat. In addition to the two distinct peaks of PCL, this pattern also shows peaks at (111), (200), (220), and (311) for Ag, according to JCPDS 04-0783, and (110) and (222) peaks for (Cu_2O), consistent with JCPDS 05-0667. Notably, the peak at 61.44° of Cu_2O has been shifted to 63.9°, and it forms another phase with Ni, which corresponds to the form (220) peak for NiO. The slight peak shifting of the nanohybrid is due to a small variation in ionic radii of Cu^{2+} and Ni^{2+}. When Ni replaces Cu in the lattice, it creates a slight compressive strain, causing the peak shift.[63,64] These peaks confirm the successful incorporation of all three metal nanohybrids into the PCL membrane. Fig. 3a(iii) depicts the XRD pattern for the T-C-PCL mat. Here (111), (200), (220), and (311) peaks indicate the presence of Ag, while (222) is for Cu_2O, and (200) peak indicates the presence of Ni nanohybrid, which is well matched with JCPDS 03-1051. The peak at 25.37° indicates the presence of curcuminoids, which confirms the successful incorporation of trimetallic nanohybrid with curcuminoids into the PCL membrane.

Subsequently, FTIR analysis was performed using the ATR mode, and the peak shifts were analyzed. There PCL membrane exhibited five characteristic peaks (Fig. 3b(i)) at 1173 cm^{-1}, 1240 cm^{-1}, 1722 cm^{-1}, 2865 cm^{-1}, and 2944 cm^{-1}. These peaks correspond to the following vibrations: –C–O–C– symmetric stretching, –C–O–C– asymmetric stretching, –C═O stretching of the ester carbonyl group, CH_2 symmetric stretching, and CH_2 asymmetric stretching vibrations respectively. Those peaks shifted to the positions shown in Fig. 3b(ii) and (iii), confirming the incorporation of trimetallic nanohybrid and curcuminoids into PCL membrane. The carbonyl band at 1722 cm^{-1} was displaced due to interaction with Ag particles.[65]

Fig. 3c depicts the Raman spectra of the PCL membrane (Fig. 3c(i)) and PCL mat, and T-C-PCL mat (Fig. 3c(ii)). The Raman spectrum of PCL displays a peak at 1720 cm^{-1}, which is associated with the methylene group. The bands at 1442 cm^{-1} and 1304 cm^{-1} are attributed to the bending vibrations of the –CH group, while the stretching vibration band of C–O–C appears at 1110 cm^{-1} and has been shifted to 1121 cm^{-1} in the T-C-PCL mat.[65] This shift could be attributed to the interaction between the PCL polymer chains and the metal nanoparticles present in the trimetallic nanohybrid. When metal nanoparticles, such as silver, copper, and nickel, are incorporated into the PCL matrix, they can form coordination bonds or interact with the polymer chains through van der Waals forces, electrostatic interactions, or other non-covalent interactions. These interactions can influence the conformational structure of the PCL chains by either stiffening or altering their flexibility, which in turn affects the local molecular environment around the C–O–C bonds. The change in conformation can cause a redistribution of electron density or strain in the polymer backbone, which modifies the vibrational frequency of the C–O–C bonds. This alteration is reflected in a shift in the Raman peak from 1110 cm^{-1} to 1121 cm^{-1}. Moreover, the presence of the metal nanoparticles could also affect the polarity of the surrounding environment, further influencing the vibrational modes of the functional groups in the polymer and leading to changes in the observed Raman spectrum. Therefore, the observed peak shift can be seen as a direct result of the interaction between the PCL matrix and the metal nanoparticles in the nanohybrid, modifying the molecular vibrations in a way that reflects these structural and electronic changes.[66,67]

According to the literature,[68] pure curcuminoids show bands in Raman spectrum at 1601 cm^{-1} and 1626 cm^{-1}, attributed to the ν(C═C) motions of the inter-ring chain and to ν(C═O)/ν(C═C) vibrations in the side aromatic rings, bands at 1431 cm^{-1} and 1495 cm^{-1}, associated to $\delta(CH_3)$ group. Those bands have been shifted to 1595 cm^{-1}, 1633 cm^{-1}, 1418 cm^{-1}, and 1489 cm^{-1} in the T-C-PCL mat, confirming the successful incorporation of curcuminoids into the PCL membrane. When comparing the Raman spectra of metal nanohybrids (Fig. S4c(ii)†), it shows Cu–O band at 614 cm^{-1}, which has been shifted to 598 cm^{-1} in Fig. 3c(ii), band at 810 cm^{-1} (Fig. S4c(i)†) and 816 cm^{-1} (Fig. S4c(iii)†) in Ag and Ni nanohybrids have been shifted to 834 cm^{-1} in T-C-PCL mat (Fig. 3c(ii)). These results confirm the successful incorporation of trimetallic nanohybrid and curcuminoids into the PCL mat.

Fabricated nanofiber membranes were morphologically analyzed using SEM. Fig. 3d and e depict the SEM images and distribution of fiber diameter of electrospun membranes. Fig. 3d(i) shows the SEM image of the PCL membrane with even morphology with an average fiber diameter 288 ± 8 nm (Fig. 3e(i)). The SEM image of the trimetallic nanohybrid incorporated in the PCL membrane is shown in Fig. 3e(ii) with an average fiber diameter 224 ± 7 nm. Fig. 3e(iii) shows the SEM image of a trimetallic nanohybrid with curcuminoids incorporated in the PCL membrane with an average fiber diameter 217 ± 7 nm (Fig. 3e(iii)). This decrement is due to the enhancement of the conductivity of the solution when guest molecules were introduced to the electrospinning solution. As the solution contains more electric charges, it causes to overcome the surface tension of the solution and can be easily thinned and stretched the nanofibers.[69]

The EDX analysis of the electrospun mats incorporated with the synthesized nanoparticles (silver, copper, and nickel) and curcumin provides important insights into the elemental composition of the mats and the interactions between the materials (Fig. S10†). Three different mats were analyzed: a PCL mat, a T-PCL mat (Ag, Cu, and Ni) mat, and a T-C-PCL mat.

In the PCL mat, the analysis revealed that the mat was composed primarily of carbon (C) and oxygen (O), with weight percentages of 68.76% and 31.24%, respectively. This composition is consistent with the chemical structure of polycaprolactone (PCL). The T-PCL mat, which contains silver (Ag), copper (Cu), and nickel (Ni), showed that copper (Cu) is the most predominant metal in the sample, with a weight percentage of 3.52%. This result suggests that copper nanoparticles were successfully incorporated into the mat, and they are present in a higher proportion compared to the other metals. The EDX also reveals high percentages of carbon (C) and oxygen (O), which were found to be 70.86% and 25.05%, respectively. These elements are likely derived from the PCL polymer used as the matrix material for the electrospinning process. The presence of these organic elements is expected, as PCL is a polymer with a significant carbon and oxygen content. The combination of these elements with the metals indicates that the trimetallic nanoparticles were successfully incorporated into the polymer matrix, with copper being the most abundant metal in the structure.

The T-C-PCL mat showed a similar trend, with copper still being the most predominant metal, present at a weight percentage of 2.64%. This is consistent with the trimetallic formulation, where copper was found to dominate among the three metals. The carbon and oxygen content in this mat is even higher than that in the trimetallic-only mat, with values of 64.31% and 31.67%, respectively. These values can be attributed to the combined presence of PCL and curcuminoids. Curcuminoids, as an organic compound, contribute significantly to the carbon and oxygen content, while the PCL polymer further adds to these values. The relatively high percentage of organic content (C and O) in this mat indicates a robust polymeric matrix that likely supports the dispersion of the metal nanoparticles and curcuminoids.

The average incorporated amount of metals throughout the mats was analyzed using AAS. For that, the fabricated mats were manually digested by a mixture of HCl and HNO_3 in a 3 : 1 ratio, and the average incorporated amount of Ag, Cu, and Ni was investigated in electrospun PCL membranes. Table 6 shows the average incorporated amount of Ag, Cu, and Ni in T-PCL mat and T-C-PCL mat.

To analyze the release of the metal nanoparticles, ICP-MS analysis was performed. The released amounts of metals are tabulated in Table 7. Those amounts were further compared with literature-reported values, which were obtained using zebra fish tests, to get an idea about the toxic concentrations of respective nanoparticles to the human body.

Table 6 Average amounts of nanoparticles in a unit area of PCL nanofiber mats

	Average amount (mg cm^{-2}) (10^{-2})	
Metal	T-PCL mat	T-C-PCL mat
Ag	0.28 ± 0.10	0.36 ± 0.18
Cu	1.30 ± 0.56	1.90 ± 0.70
Ni	0.22 ± 0.02	0.08 ± 0.01

Table 7 Released amounts of nanoparticles from 3 cm × 3 cm area of PCL nanofiber mats

	Released amount (μg L^{-1})	
Metal	T-PCL mat	T-C-PCL mat
Ag	4.80	3.00
Cu	180	189
Ni	38.3	19.0

Studies have shown that the toxic effect of Ag nanoparticles might be more serious when the concentration increases up to 3 mg L^{-1} or higher. Cu nanoparticles can be acutely toxic within a 1–1.5 mL L^{-1} concentration. The toxic concentration of Ni nanoparticles is reported as >115 mg L^{-1}. Therefore, it can be concluded that although the nanoparticles were released from the membrane, those values are much lower than the reported LD_{50} values. So, it can be confirmed that these can be used as wound dressings as there is no toxicity for the human body. However, the toxicity varies with the nanoparticle size, where smaller particles usually have higher toxicity.[70,71]

3.10 Incorporated amounts and encapsulation efficiency of curcuminoids in fiber mats

The average incorporated amounts of curcuminoids in T-C-PCL mat and in C-PCL mat were calculated using the calibration plot (Fig. S1(b)†) and absorbance values at 427 nm wavelength. The average mass of curcuminoids in a 1 cm × 1 cm piece was calculated as 0.184 ± 0.02 mg and 0.449 ± 0.16 mg in T-C-PCL mat and in C-PCL mat, respectively. Considering the actual and theoretical content of curcuminoids in mats, the encapsulation efficiency was calculated as 67.63% and 74.13%, respectively.

3.11 Release behavior of curcuminoids from T-C-PCL mat

Fig. 4 depicts the (a) cumulative release percentage of curcuminoids against time and (b) release kinetics of curcuminoids from T-C-PCL mat. According to Fig. 4a, the burst release of curcuminoids can be observed for 480 minutes (8 hours) and then reaches an almost constant level over 72 hours, which confirms the slow and sustained release of the drug. The release mechanism of curcuminoids was investigated referring to four different kinetic models; zeroth order, first order, Higuchi model, and Korsmeyer-Peppas model. From the best fit curves, R^2 values were obtained. Zeroth-order model provided the highest R^2 value, suggesting that the release of curcuminoids occurred in a slow and sustainable manner. Also, it can be further concluded that the rate of release mechanism does not depend on curcuminoids concentration, and it is a function of time.[72] Higher value of the Higuchi model also suggests the release mechanism follows more than one mechanism.[73] However, the release amount of curcuminoids was over 45% after 24 hours, indicating the long-term release for practical applications, such as wound dressings.

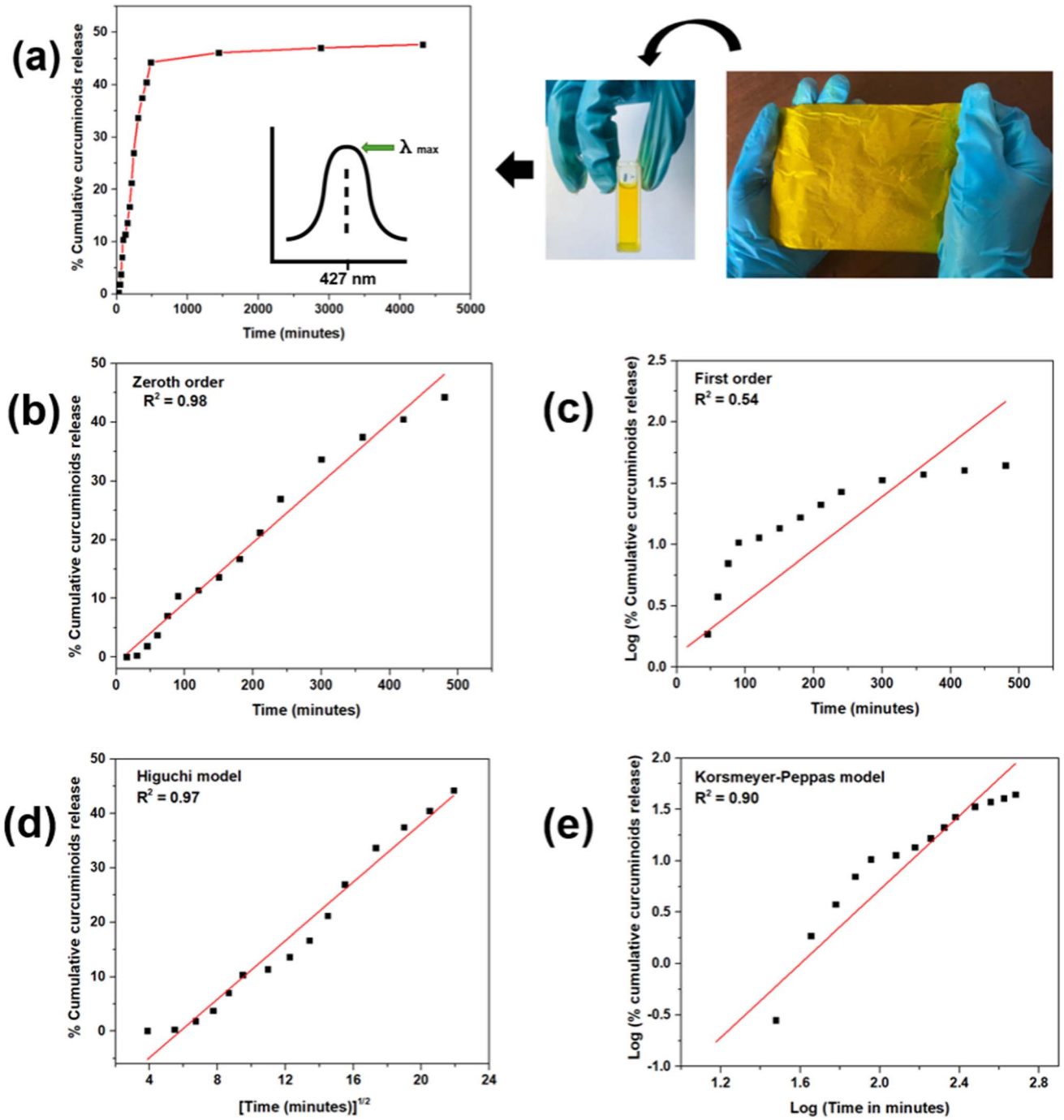

Fig. 4 (a) Cumulative release of curcuminoids from T-C-PCL mat and release kinetics of curcuminoids according to different kinetics models; (b) zeroth order, (c)first order, (d) Higuchi model and (e) Korsmeyer-Peppas model.

3.12 DPPH assay for evaluating the radical scavenging activity of fabricated nanofiber mats

As shown in Fig. 5, T-C-PCL mat exhibits the highest % radical scavenging activity (76.14 ± 0.99%), compared to other nanofiber mats, because of the synergism between different metal nanoparticles and natural antioxidant, curcuminoids. T-PCL mat exhibits the % radical scavenging activity of 68.79 ± 0.16%. Whereas the C-PCL mat shows a comparable % radical scavenging activity of 44.88 ± 0.05%.

A statistical analysis was then performed to confirm that there is a significant difference between mean values of % radical scavenging activities of C-PCL mat, T-PCL mat, and PCL mat with T-C-PCL (Ag + Cu + Ni + Curcuminoids) mat at the significance level of 0.05 (Fig. S11†). The calculated *p* values are lower than the employed significance level of 0.05. Therefore, it can be interpreted that there is a significant difference between the mean values of % radical scavenging activities of C-PCL mat, T-PCL mat, and PCL mat with T-C-PCL mat at the significance

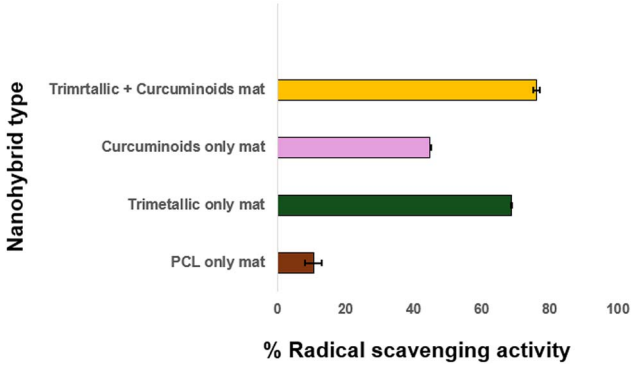

Fig. 5 Radical scavenging activity of fabricated metal nanohybrid incorporated PCL nanofiber mats.

level of 0.05, when equal variance is assumed. The samples were further supported by analysis of variance (ANOVA) using MINITAB 18, and the significant difference of each sample was analyzed by Tukey pairwise comparison at the significance level of 0.05, and they were significantly different according to Tukey pairwise comparison. Table S2† depicts the significant difference of each sample.

3.13 Evaluation of the antimicrobial activity for the electrospun nanofiber mats

Finally, a disc diffusion experiment was utilized to determine the synergistic antimicrobial activity of metal NPs-curcuminoids based nanohybrids incorporating a nanofiber mat. This disc diffusion assay shows how well an antibiotic therapy works against specific microbes. It is predicted that the inhibitory zones surrounding the discs that were placed on the surface of the agar plates. Here, we initially employed the disc diffusion assay on previously selected ATCC strains of microorganisms, including bacteria and fungi. The inhibition zones of the several nanofiber mats against the ATCC strains of test microbes are displayed in Fig. 6(i), which lists the inhibition zone values that different nanofiber mats have displayed in Table 8.

A statistical analysis was then performed to confirm that there is a significant difference between the zones of inhibition of T-PCL mat, C-PCL mat, and the T-C-PCL mat-based nanohybrid incorporated PCL mat at the significance level of 0.05. Fig. 6 shows the respective zones of inhibition and evaluates significant differences. The reported p values are lower than the employed significance level of 0.05. Hence, it can be interpreted that there is a significant difference between the mean values of inhibition zones of T-PCL mat and T-C-PCL mat based nanohybrid incorporated PCL mat, and between C-PCL mat and T-C-PCL mat at the significance level of 0.05, when equal variance is assumed. The assays for clinical isolates of ATCC strains and quality control strains of the examined microbes were conducted to proceed with the disc diffusion assay.

Considering the results, the highest antimicrobial activity was shown by T-C-PCL mat. T-PCL mat exhibited the lowest zone of inhibition against all the test strains of microbes. The T-C-0PCL mat-based nanohybrid incorporated PCL mat showed the highest zone of inhibition against all the test microorganisms. When analyzing the zones of inhibition, it is clearly evident that the T-C-PCL mat showed a synergistic antimicrobial activity against both gram-positive and gram-negative bacteria and against fungi as well. The conventional treatments require specific antibiotic agents for treating the specific types of microbes, including gram-positive bacteria (erythromycin was used), gram-negative bacteria (Merepenem was used), and fungi (fluconazole was used).

However, in this study, the T-C-PCL mat showed an antimicrobial activity against all the tested microbes while covering a broad spectrum of microorganisms. Regarding the antifungal activity of the fabricated mats, they are also in good agreement with the results for bacteria. The highest antifungal activity was shown by the T-C-PCL mat. This is an important finding as some skin rashes are mainly due to this yeast, *Candida albicans*. Candida is a commensal that resides on our skin and causes opportunistic infections such as Candida skin infection and vaginal Candidiasis. Considering the antibacterial activity and the antifungal activity, it can be clearly observed that the T-C-PCL mat exhibits greater antifungal activity than antibacterial activity. This observation is in good agreement with the results of the well diffusion assay, which was previously conducted for the nanohybrid powders. The metal nanoparticle Ni may be the reason that boosts the antifungal activity because it has the lowest diameter. These dimensions facilitate the penetration of cell membranes. Fungal cells are eukaryotic cells, which means they have a well-organized cellular structure with a nucleus, when compared with bacterial cells because bacteria are prokaryotic cells. Even though the cellular structure is complex, the invented T-C-PCL mat can combat these yeast-type fungal cells as well.[74,75]

However, according to the reported results, T-C-PCL mat will be a potential new hope for the development of emerging applications in the biomedical field, such as wound dressings against a broad spectrum of microbes including gram-positive and gram-negative bacteria and yeast-type fungi. The integration of broad-spectrum antimicrobial activity with sustainability focuses on utilizing natural compounds and nanomaterials that effectively combat a wide range of pathogens while reducing environmental impact and preventing resistance development.

According to the published literature, Mosallanezhad *et al.*[76] demonstrated that PCL/chitosan nanofibers loaded with curcumin and ZnO exhibited notable antibacterial activity, inhibiting *E. coli* and *S. aureus* by 49.2 ± 5.8% and 59.3 ± 3.9%, respectively, aligning with the trends observed in our fiber-embedded formulations. Sedghi *et al.*[77] achieved up to 94% inhibition of methicillin-resistant *S. aureus* using a chitosan/curcumin/fGO nanofiber system, underscoring the potential of curcumin-metal synergy. Moreover, Ranjbar-Mohammadi *et al.*[78] reported significant wound healing in diabetic rat models using PCL/gum tragacanth/curcumin fibers, with enhanced re-epithelialization and collagen deposition within 15 days. Similarly, Khan *et al.*[79] used PLGA/silk fibroin fibers with ZnO to improve granulation tissue formation and angiogenesis.

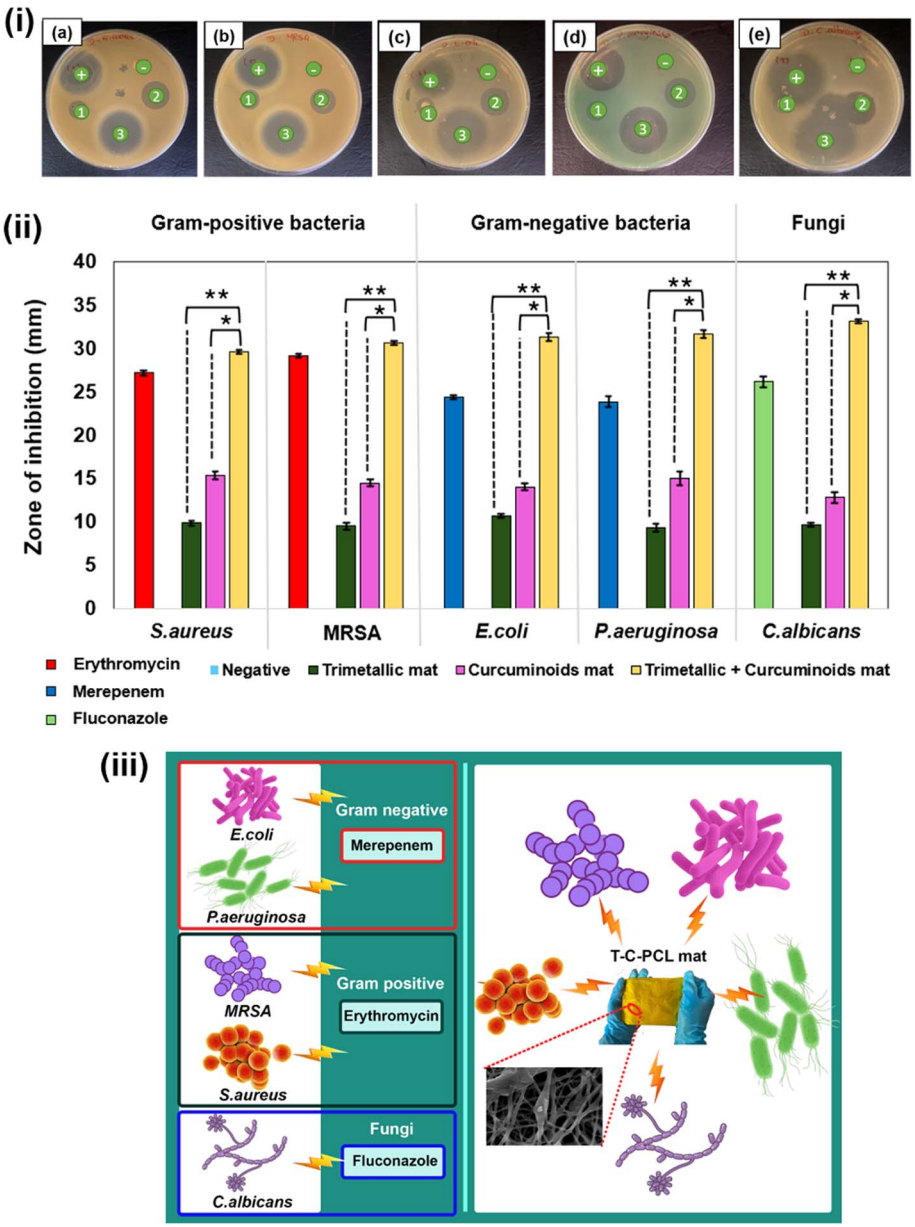

Fig. 6 (i) The zone of inhibition of (a). *S. aureus* (b). MRSA (c). *E-coli* (d). *P. aeruginosa* (e). *C. albicans*; (+) positive control, (−) negative control, (1) T-PCL mat, (2) C-PCL mat and (3) T-C-PCL mat. (ii) The inhibition zone values of different nanofiber mats against ATCC cultures of microbes; the significant difference between (**) C-PCL mat with T-C-PCL mat and (*) T-PCL mat with T-C-PCL mat. (iii) Significance of T-C-PCL mat as a broad-spectrum antimicrobial agent.

Table 8 The zones of inhibition against tested microbes by the nanohybrids incorporated PCL mats (1) T-PCL mat, (2) C-PCL mat and (3) T-C-PCL mat[a]

	Microorganism				
Inhibition zone (mm)	*S. aureus*	MRSA	*E. coli*	*P. aeruginosa*	*C. albicans*
Positive (+)	27.17 ± 0.24^{a}	29.17 ± 0.24^{a}	24.33 ± 0.24^{a}	23.83 ± 0.62^{a}	26.17 ± 0.62^{a}
Negative (−)	0.00 ± 0.00^{b}	0.00 ± 0.00^{b}	0.00 ± 0.00^{b}	0.00 ± 0.00^{b}	0.00 ± 0.00^{b}
1	9.83 ± 0.24^{c}	9.50 ± 0.41^{c}	10.67 ± 0.24^{c}	9.33 ± 0.47^{c}	9.67 ± 0.24^{c}
2	15.33 ± 0.47^{d}	14.50 ± 0.41^{d}	14.00 ± 0.41^{d}	15.00 ± 0.82^{d}	12.83 ± 0.62^{d}
3	29.67 ± 0.24^{e}	30.67 ± 0.24^{e}	31.33 ± 0.47^{e}	31.67 ± 0.47^{e}	33.17 ± 0.24^{e}

[a] Values followed by different superscripts in the same column are significantly different ($P < 0.05$) according to Tukey's pairwise comparison test ($n = 3$).

While these studies confirm the dual antibacterial and regenerative capabilities of curcumin-metal nanofiber systems, our study is, to our knowledge, the first to integrate a trimetallic (Ag–Cu–Ni) nanohybrid with curcuminoids derived specifically from turmeric oleoresin into a biodegradable electrospun PCL membrane. This system not only demonstrates robust antimicrobial and anti-inflammatory activity but also advances the field through its sustainable, eco-conscious design and enhanced therapeutic potential, addressing both biomedical and environmental safety challenges in a single platform.

4 Conclusion

In this study, we have successfully developed a novel antimicrobial electrospun polymeric membrane that combines trimetallic nanoparticles (Ag, Cu, Ni) with turmeric oleoresin and curcuminoids, demonstrating exceptional synergistic antimicrobial and anti-inflammatory properties. The incorporation of these metal-curcuminoids based nanohybrids into a polycaprolactone (PCL) electrospun mat not only enhances its antimicrobial efficacy against a broad spectrum of microbes, including resistant strains, but also imparts additional biological benefits, such as anti-inflammatory activity through curcumin. It exhibited maximum values for inhibition zones ranging from 29.67 $\pm$ 0.24 to 33.17 $\pm$ 0.24 mm against all the tested microbes. These results confirmed the broad-spectrum activity of the T-C-PCL mat against gram-positive bacteria, gram-negative bacteria, and yeast-type fungi. The radical scavenging activity (RSA) is believed to be the main antimicrobial mechanism of these nanofiber mats, and it has recorded the maximum value of RSA 76.14 $\pm$ 0.99% for T-C-PCL mat. Additionally, the curcuminoids in the nanohybrids showed potent anti-inflammatory activity that exhibited the maximum anti-inflammatory action of 72.81 $\pm$ 0.33% for 5000 ppm concentration. The development of this electrospun nanohybrid membrane exemplifies the potential of sustainable biomaterials and technologies in the design of effective antimicrobial treatments. By leveraging biodegradable materials and incorporating natural antimicrobial agents like curcuminoids, this product provides a green alternative to conventional methods, reducing environmental impact. This approach not only addresses the growing concern of antimicrobial resistance but also paves the way for more sustainable, eco-friendly, and cost-effective solutions in healthcare and safety applications. With its dual functionality as both a physical and biological barrier, this antimicrobial electrospun membrane holds great potential in addressing current challenges in the management of microbial infections, following appropriate toxicity assays through *in vivo* animal studies. The integration of broad-spectrum antimicrobial activity with sustainability offers an exciting opportunity to utilize natural compounds with nanomaterials that effectively target a wide range of pathogens. By adopting these solutions, we can enhance public health while minimizing environmental impact and addressing the challenge of resistance development. This approach fosters a healthier balance between human needs and environmental stewardship.

While this study demonstrates the promising antimicrobial and anti-inflammatory performance of trimetallic–curcuminoid nanohybrids embedded in electrospun PCL membranes, several aspects warrant further investigation. The current work is limited to *in vitro* assessments; therefore, future studies should include comprehensive *in vivo* evaluations to better understand biocompatibility, tissue integration, long-term degradation behavior, and therapeutic efficacy in relevant animal wound models. Additionally, exploring the mechanistic interactions between the trimetallic system and biological targets, such as bacterial membranes or inflammatory pathways, could provide deeper insight into the synergistic effects observed. Scaling up the fabrication process while maintaining reproducibility and consistency is also an essential step toward potential clinical translation. Moreover, future research could investigate the controlled release kinetics of curcuminoids and metal ions, as well as the potential integration of other bioactive agents or stimuli-responsive elements to broaden the scope of biomedical applications. These directions will help bridge the gap between laboratory findings and real-world clinical implementation, advancing the development of sustainable and multifunctional biomaterials.

Data availability

All data produced and analyzed in this research are included in this manuscript.

Author contributions

Dinithi Senanayake – conduct the experiment, formal analysis of data and writing the manuscript. Piumika Yapa – conduct microbiology experiments, formal analysis of data and writing the manuscript. Sanduni Dabare – conduct the experiment, formal analysis of data and writing the manuscript. Imalka Munaweera – conceptualization, funding acquisition, methodology, supervision, writing, review and editing the original draft. Manjula M. Weerasekera – supervision and curation of microbiology data, review and editing the original draft. Thusitha N. B. Etampawala – supervision and curation of characterization data, review and editing the original draft. Maheshika Sethunga – methodology of the curcumin extraction, review and editing the original draft. Dinesh Attygalle – supervision and curation of characterization data (SEM and EDAX analysis), review and editing the original draft. Shantha Amarasinghe – supervision and curation of characterization data (SEM and EDAX analysis), review and editing the original draft. All authors have approved the final version of the manuscript.

Conflicts of interest

The authors declare that there is no conflict of interest.

Acknowledgements

Financial support for this study is acknowledged by the University of Sri Jayewardenepura, Sri Lanka under the research

grant number ASP/01/RE/SCI/2022/15 and The World Academy of Science (20/102/RG/CHE/AS_1 – FR3240314134) for providing grants for the electrospinning setup. Authors acknowledge the Instrument Centre, Faculty of Applied Sciences, University of Sri Jayewardenepura for the facility provided in analysis and characterization.

References

1 J. Whitlow, S. Pacelli and A. Paul, Polymeric nanohybrids as a new class of therapeutic biotransporters, *Macromol. Chem. Phys.*, 2016, **217**(11), 1245–1259, DOI: **10.1002/macp.201500464**.

2 N. Zhao, L. Yan, X. Zhao, X. Chen, A. Li, D. Zheng, *et al.*, Versatile types of Organic/Inorganic nanohybrids: from strategic design to biomedical applications, *Chem. Rev.*, 2018, **119**(3), 1666–1762, DOI: **10.1021/acs.chemrev.8b00401**.

3 N. Aich, J. Plazas-Tuttle, J. R. Lead and N. B. Saleh, A critical review of nanohybrids: synthesis, applications and environmental implications, *Environ. Chem.*, 2014, **11**(6), 609, DOI: **10.1071/en14127**.

4 S. Prakash, M. Malhotra, W. Shao, C. Tomaro-Duchesneau and S. Abbasi, Polymeric nanohybrids and functionalized carbon nanotubes as drug delivery carriers for cancer therapy, *Adv. Drug Delivery Rev.*, 2011, **63**(14–15), 1340–1351, DOI: **10.1016/j.addr.2011.06.013**.

5 E. Sánchez-López, D. Gomes, G. Esteruelas, L. Bonilla, A. L. Lopez-Machado, R. Galindo, *et al.*, Metal-Based nanoparticles as antimicrobial agents: An overview, *Nanomaterials*, 2020, **10**(2), 292, DOI: **10.3390/nano10020292**.

6 B. S. Medic, N. Tomic, N. Lagopati, M. Gazouli and L. Pojskic, Advances in metal and metal oxide nanomaterials for topical antimicrobial applications: Insights and future perspectives, *Molecules*, 2024, **29**(23), 5551, DOI: **10.3390/molecules29235551**.

7 Y. N. Slavin, J. Asnis, U. O. Häfeli and H. Bach, Metal nanoparticles: understanding the mechanisms behind antibacterial activity, *J. Nanobiotechnol.*, 2017, **15**(1), 65, DOI: **10.1186/s12951-017-0308-z**.

8 J. Díaz-Visurraga, C. Gutierrez, C. von Plessing and A. García, *Metal Nanostructures as Antibacterial Agents, Science against Microbial Pathogens: Communicating Current Research and Technological Advances*, vol. **1**(5), pp. 210–218.

9 C. Bankier, R. K. Matharu, Y. K. Cheong, G. G. Ren, E. Cloutman-Green and L. Ciric, Synergistic antibacterial effects of metallic nanoparticle combinations, *Sci. Rep.*, 2019, **9**(1), 16074, DOI: **10.1038/s41598-019-52473-2**.

10 J. A. Garza-Cervantes, A. Chávez-Reyes, E. C. Castillo, G. García-Rivas, O. A. Ortega-Rivera, E. Salinas, *et al.*, Synergistic antimicrobial effects of Silver/Transition-Metal combinatorial treatments, *Sci. Rep.*, 2017, **7**(1), DOI: **10.1038/s41598-017-01017-7**.

11 D. V. Francis, M. N. Jayakumar, H. Ahmad and T. Gokhale, Antimicrobial activity of biogenic metal oxide nanoparticles and their synergistic effect on clinical pathogens, *Int. J. Mol. Sci.*, 2023, **24**(12), 9998, DOI: **10.3390/ijms24129998**.

12 Y. Hussain, W. Alam, H. Ullah, M. Dacrema, M. Daglia, H. Khan, *et al.*, Antimicrobial potential of curcumin: therapeutic potential and challenges to clinical applications, *Antibiotics*, 2022, **11**(3), 322, DOI: **10.3390/antibiotics11030322**.

13 S. Mošovská, P. Petáková, M. Kaliňák and A. Mikulajová, Antioxidant properties of curcuminoids isolated from Curcuma longa L, *Acta Chim. Slovaca*, 2016, **9**(2), 130–135, DOI: **10.1515/acs-2016-0022**.

14 G. K. Jayaprakasha, B. S. Jena, P. S. Negi and K. K. Sakariah, Evaluation of Antioxidant Activities and Antimutagenicity of Turmeric Oil: A Byproduct from Curcumin Production, *Z. Naturforsch. C*, 2002, **57**(9–10), 828–835, DOI: **10.1515/znc-2002-9-1013**.

15 S. Honda, F. Aoki, H. Tanaka, H. Kishida, T. Nishiyama, S. Okada, *et al.*, Effects of ingested turmeric oleoresin on glucose and lipid metabolisms in obese diabetic mice: a DNA microarray study, *J. Agric. Food Chem.*, 2006, **54**(24), 9055–9062, DOI: **10.1021/jf061788t**.

16 S. Prasad, D. DuBourdieu, A. Srivastava, P. Kumar and R. Lall, Metal–Curcumin complexes in therapeutics: An approach to enhance pharmacological effects of curcumin, *Int. J. Mol. Sci.*, 2021, **22**(13), 7094, DOI: **10.3390/ijms22137094**.

17 A. A. Targhi, N. Mousavi-Niri, F. J. Ansari and H. J. Mansoorian, The antibacterial effects of Curcumin-Silver nanoparticle and Curcumin-Copper nanoparticle loaded niosomes, *Health Dev. J.*, 2022, **11**(1), 1–8, DOI: **10.34172/jhad.2022.92066**.

18 K. K. Sarwa, Potential of ligand conjugated metallic nanoparticles in the treatment of carcinoma in the delivery of Plant-Derived payload, *Asian J. Pharm.*, 2024, **18**, 04, DOI: **10.22377/ajp.v18i04.5829**.

19 F. Ghiselli, R. Majer, A. Piva and E. Grilli, Activation of cannabinoid receptor 2 by turmeric oleoresin reduces inflammation and oxidative stress in an osteoarthritis in vitro model, *Front. Pharmacol*, 2024, 15, DOI: **10.3389/fphar.2024.1488254**.

20 L. Péret-Almeida, C. C. Naghetini, E. Nunan, R. Junqueira and M. Glória, In vitro antimicrobial activity of the ground rhizome, curcuminoid pigments and essential oil of Curcuma longa L, **https://api.semanticscholar.org/CorpusID:90788512**.

21 I. Maliszewska and T. Czapka, Electrospun Polymer Nanofibers with Antimicrobial Activity, *Polymers*, 2022, **14**(9), 1661, DOI: **10.3390/polym14091661**.

22 S. Kumarage, I. Munaweera and N. Kottegoda, A comprehensive review on electrospun nanohybrid membranes for wastewater treatment, *Beilstein J. Nanotechnol.*, 2022, **13**, 137–159, DOI: **10.3762/bjnano.13.10**.

23 L. Pisklákova, K. Skuhrovcová, T. Bártová, J. Seidelmannová, Š. Vondrovic and V. Velebný, Trends in the Incorporation of Antiseptics into Natural Polymer-Based Nanofibrous Mats, *Polymers*, 2024, **16**(5), 664, DOI: **10.3390/polym16050664**.

24 N. Ditaranto, F. Basoli, M. Trombetta, N. Cioffi and A. Rainer, Electrospun nanomaterials implementing antibacterial inorganic nanophases, *Appl. Sci.*, 2018, **8**(9), 1643, DOI: 10.3390/app8091643.

25 S. Jiang, X. Liao and H. Hou, in *Improvement on Mechanical Property of Electrospun Nanofibers, Their Yarns, and Materials*, CRC Press eBooks, 2019, pp. 212–242, DOI: 10.1201/9780429085765-7.

26 M. Zhang, W. Song, Y. Tang, X. Xu, Y. Huang and D. Yu, Polymer-Based Nanofiber–Nanoparticle hybrids and their medical applications, *Polymers*, 2022, **14**(2), 351, DOI: 10.3390/polym14020351.

27 S. Mahira, A. Jain, W. Khan and A. J. Domb, in *Antimicrobial Materials—An Overview*, The Royal Society of Chemistry eBooks, 2019, pp. 1–37, DOI: 10.1039/9781788012638-00001.

28 S. Shafaei, M. Lackner, R. Voloshchuk, I. Voloshchuk, J. Guggenbichler and C. Zollfrank, Innovative development in antimicrobial inorganic materials, *Recent Pat. Mater. Sci.*, 2014, **7**(1), 26–36, DOI: 10.2174/1874464806666131204235326.

29 C. Madhusha, K. Rajapaksha, I. Munaweera, M. De Silva, C. Perera, G. Wijesinghe, *et al.*, A novel green approach to synthesize Curcuminoid-Layered double hydroxide nanohybrids: adroit biomaterials for future antimicrobial applications, *ACS Omega*, 2021, **6**(14), 9600–9608, DOI: 10.1021/acsomega.1c00151.

30 H. A. Pawar, A. J. Gavasane and P. D. Choudhary, A Novel and Simple Approach for Extraction and Isolation of Curcuminoids from Turmeric Rhizomes, *Advances in Recycling & Waste Management*, 2018, **06**, 01, DOI: 10.4172/2475-7675.1000300.

31 C. Madhusha, K. Rajapaksha, I. Munaweera, M. De Silva, C. Perera, G. Wijesinghe, *et al.*, A novel green approach to synthesize Curcuminoid-Layered double hydroxide nanohybrids: adroit biomaterials for future antimicrobial applications, *ACS Omega*, 2021, **6**(14), 9600–9608, DOI: 10.1021/acsomega.1c00151.

32 H. Rajapaksha, et al.) 'Evaluation of in vitro anti-inflammatory activity and in-silico pharmacokinetics and molecular docking study of Horsfieldia Iryaghedhi, *J. Phytopharm.*, 2024, **13**(2), 143–153, DOI: 10.31254/phyto.2024.13208.

33 A. M, M. I. Arumugham, K. Ramalingam and R. S, Evaluation of the anti-inflammatory, antimicrobial, antioxidant, and cytotoxic effects of Chitosan Thiocolchicoside-Lauric acid Nanogel, *Cureus*, 2023, **15**(9), e46003, DOI: 10.7759/cureus.46003.

34 M. Kushwah, S. Bhadauria, K. Arora and M. S. Gaur, Enhanced catalytic activity of chemically synthesized Au/Ag/Cu trimetallic nanoparticles, *Mater. Res. Express*, 2019, **6**(9), 095013, DOI: 10.1088/2053-1591/ab2b04.

35 S. Alam, S. Ullah, M. Ilyas, N. U. Rehman, M. Zahoor, M. N. Umar, *et al.*, Silver, copper, and cobalt trimetallic nanoparticles; synthesis, characterization and its application as adsorbent for acid blue 7 dye, *Z. Phys. Chem.*, 2023, **237**(12), 2037–2053, DOI: 10.1515/zpch-2023-0370.

36 I. Munaweera and M. L. C. Madhusha, *Characterization Techniques for Nanomaterials*, CRC Press, Boca Raton, 2023.

37 N. C. De S Santos, L. S. R. B. De, D. C. Leal, S. M. D. Prado, D. F. Micheletti, E. G. Sampiron, *et al.*, Determination of minimum bactericidal concentration, in single or combination drugs, against Mycobacterium tuberculosis, *Food Res. Int.*, 2020, **15**(2), 107–114, DOI: 10.2217/fmb-2019-0050.

38 P. N. Yapa, I. Munaweera, M. M. Weerasekera and L. Weerasinghe, Nanoarchitectonics for synergistic activity of multimetallic nanohybrids as a possible approach for antimicrobial resistance (AMR), *J. Biol. Inorg. Chem.*, 2024, **29**(5), 477–498, DOI: 10.1007/s00775-024-02066-w.

39 CLSI, *Performance Standards for Antimicrobial Disk and Dilution Susceptibility Tests for Bacteria Isolated from Animals: Approved Standard*, Clinical & Laboratory Standards Institute, 2nd edn, 2002, vol. 22(6).

40 M. Balouiri, M. Sadiki and S. K. Ibnsouda, Methods for in vitro evaluating antimicrobial activity: a review, *J. Pharm. Anal.*, 2016, **6**(2), 71–79, DOI: 10.1016/j.jpha.2015.11.005.

41 C. A. Marin-Flores, O. Rodríguez-Nava, M. García-Hernandez, R. Ruiz-Guerrero, F. Juarez-Lopez and A. de J. Morales-Ramírez, Free-radical scavenging activity properties of ZnO sub-micron particles: size effect and kinetics, *J. Mater. Res. Technol.*, 2021, **13**, 1665–1675, DOI: 10.1016/j.jmrt.2021.05.050.

42 K. S. Athira, P. Sanpui and K. Chatterjee, Fabrication of Poly(Caprolactone) nanofibers by electrospinning, *J. Polym. Biopolym. Phys. Chem.*, 2014, **2**(4), 62–66.

43 P. Yapa, I. Munaweera, M. M. Weerasekera and L. Weerasinghe, Synergistic antimicrobial nanofiber membranes based on metal incorporated silica nanoparticles as advanced antimicrobial layers, *RSC Adv.*, 2024, **14**(46), 33919–33940, DOI: 10.1039/d4ra05052e.

44 A. Alehosseini, L. G. Gómez-Mascaraque, M. Martínez-Sanz and A. López-Rubio, Electrospun curcumin-loaded protein nanofiber mats as active/bioactive coatings for food packaging applications, *Food Hydrocolloids*, 2019, **87**, 758–771, DOI: 10.1016/j.foodhyd.2018.08.056.

45 M. M. Mahmud, S. Zaman, A. Perveen, R. A. Jahan, M. F. Islam and M. T. Arafat, Controlled release of curcumin from electrospun fiber mats with antibacterial activity, *J. Drug Delivery Sci. Technol.*, 2019, **55**, 101386, DOI: 10.1016/j.jddst.2019.101386.

46 A. A. Targhi, A. Moammeri, E. Jamshidifar, K. Abbaspour, S. Sadeghi, L. Lamakani, *et al.*, Synergistic effect of curcumin-Cu and curcumin-Ag nanoparticle loaded niosome: Enhanced antibacterial and anti-biofilm activities, *Bioorg. Chem.*, 2021, **115**, 105116, DOI: 10.1016/j.bioorg.2021.105116.

47 S. Antony, S. Elumalai and M. Benny, Isolation purification and identification of curcuminoids from turmeric (Curcuma longa L.) by column chromatography, *J. Exp. Sci.*, 2011, **2**, 21–25.

48 K. Thvar, Characterization of the purity of curcumin extraction: Comparative study of UV spectrophotometry and HPLC from a field application perspective, https://

nhsjs.com/2012/characterization-of-the-purity-of-curcumin-extraction-comparative-study-of-uv-spectrophotometry-and-high-performance-liquid-chromatography-from-a-field-application-perspective.

49 Z. Sayyar and H. J. Malmiri, Photocatalytic and antibacterial activities study of prepared self-cleaning nanostructure surfaces using synthesized and coated ZnO nanoparticles with Curcumin nanodispersion, *Z. Kristallogr. Cryst. Mater.*, 2018, **234**(5), 307–328, DOI: 10.1515/zkri-2018-2096.

50 E. H. Ismail, D. Y. Sabry, H. Mahdy and M. M. H. Khalil, Synthesis and Characterization of some Ternary Metal Complexes of Curcumin with 1,10-phenanthroline and their Anticancer Applications, *J. Sci. Res.*, 2014, **6**(3), 509–519, DOI: 10.3329/jsr.v6i3.18750.

51 A. Lanje, S. Sharma and R. Pode, Synthesis of silver nanoparticles: A safer alternative to conventional antimicrobial and antibacterial agents, *J. Chem. Pharm. Res.*, 2010, **2**, 478–483.

52 S. E. Peiris, K. L. Seneviratne, R. P. A. Shashikala, C. N. Peiris, M. I. Imalka and Y. P. Piumika, In vitro evaluation of antibacterial activity of copper and sulfur nanoparticles for controlling bacterial blight caused by Xanthomonas sp. In Anthurium andraeanum Lind, *SLIIT J. Hum. Sci.*, 2022, **3**(1), 46–55.

53 I. P. Madhushika, P. Yapa, I. Munaweera, C. Sandaruwan and M. M. Weerasekera, The antimicrobial synergy of polymer based nanofiber mats reinforced with antioxidants intercalated layered double hydroxides as a potential active packaging material, *Nano Express*, 2024, **5**(2), 025018, DOI: 10.1088/2632-959x/ad4a95.

54 A. Umer, S. Naveed, N. Ramzan, M. S. Rafique and M. Imran, A green method for the synthesis of Copper Nanoparticles using L-ascorbic acid, *Matéria (Rio J.)*, 2014, **19**(3), 197–203, DOI: 10.1590/s1517-70762014000300002.

55 G. Singh, B. P. Mohanty and G. S. S. Saini, Structure, spectra and antioxidant action of ascorbic acid studied by density functional theory, Raman spectroscopic and nuclear magnetic resonance techniques, *Spectrochim. Acta, Part A*, 2015, **155**, 61–74, DOI: 10.1016/j.saa.2015.11.005.

56 A. Khan, A. Rashid, R. Younas and R. Chong, A chemical reduction approach to the synthesis of copper nanoparticles, *Int. Nano Lett.*, 2015, **6**(1), 21–26, DOI: 10.1007/s40089-015-0163-6.

57 L. Wang, X. Yang, Q. Wang, Y. Zeng, L. Ding and W. Jiang, Effects of ionic strength and temperature on the aggregation and deposition of multi-walled carbon nanotubes, *J. Environ. Sci.*, 2016, **51**, 248–255, DOI: 10.1016/j.jes.2016.07.003.

58 S. S. Khan, A. Mukherjee and N. Chandrasekaran, Impact of exopolysaccharides on the stability of silver nanoparticles in water, *Water Res.*, 2011, **45**(16), 5184–5190, DOI: 10.1016/j.watres.2011.07.024.

59 P. Wang, Aggregation of TIO_2 nanoparticles in aqueous media: effects of pH, ferric ion and humic acid, *International Journal of Environmental Sciences & Natural Resources*, 2017, **1**, 5, DOI: 10.19080/ijesnr.2017.01.555575.

60 Z. Zachariah, R. M. Espinosa-Marzal, N. D. Spencer and M. P. Heuberger, Stepwise collapse of highly overlapping electrical double layers, *Phys. Chem. Chem. Phys.*, 2016, **18**(35), 24417–24427, DOI: 10.1039/c6cp04222h.

61 N. F. A. Rahim, N. Muhammad, N. Abdullah, B. A. Talip and N. J. S. Dusuki, Synergistic effect of polyherbal formulations on DPPH radical scavenging activity, *J. Sci. Technol.*, 2018, **10**, 2, DOI: 10.30880/jst.2018.10.02.019.

62 E. M. Abdelrazek, A. M. Hezma, A. El-Khodary and A. M. Elzayat, Spectroscopic studies and thermal properties of PCL/PMMA biopolymer blend, *Egypt. J. Basic Appl. Sci.*, 2015, **3**(1), 10–15, DOI: 10.1016/j.ejbas.2015.06.001.

63 L. Arun, C. Karthikeyan, D. Philip, M. Sasikumar, E. Elanthamilan, J. P. Merlin and C. Unni, Effect of Ni2+ doping on chemocatalytic and supercapacitor performance of biosynthesized nanostructured CuO, *J. Mater. Sci.: Mater. Electron.*, 2018, **29**(24), 21180–21193, DOI: 10.1007/s10854-018-0268-6.

64 M. P. Kumar, G. Murugadoss and M. R. Kumar, Synthesis and characterization of CuO–NiO nanocomposite: highly active electrocatalyst for oxygen evolution reaction application, *J. Mater. Sci.: Mater. Electron.*, 2020, **31**(14), 11286–11294, DOI: 10.1007/s10854-020-03677-0.

65 E. Ramírez-Cedillo, W. Ortega-Lara, M. R. Rocha-Pizaña, J. A. Gutierrez-Uribe, A. Elías-Zúñiga and C. A. Rodríguez, Electrospun polycaprolactone fibrous membranes containing Ag, TiO_2 and Na_2Ti_6O13 particles for potential use in bone regeneration, *Membranes*, 2019, **9**(1), 12, DOI: 10.3390/membranes9010012.

66 G. Mutlu, S. Calamak, K. Ulubayram and E. Guven, Curcumin-loaded electrospun PHBV nanofibers as potential wound-dressing material, *J. Drug Delivery Sci. Technol.*, 2017, **43**, 185–193, DOI: 10.1016/j.jddst.2017.09.017.

67 K. Karakas, A. Celebioglu, M. Celebi, T. Uyar and M. Zahmakiran, Nickel nanoparticles decorated on electrospun polycaprolactone/chitosan nanofibers as flexible, highly active and reusable nanocatalyst in the reduction of nitrophenols under mild conditions, *Appl. Catal., B*, 2017, **203**, 549–562, DOI: 10.1016/j.apcatb.2016.10.020.

68 A. I. Quilez-Molina, S. Barroso-Solares, V. Hurtado-García, J. A. Heredia-Guerrero, M. L. Rodriguez-Mendez, M. Á. Rodríguez-Pérez, *et al.*, Encapsulation of Copper Nanoparticles in Electrospun Nanofibers for Sustainable Removal of Pesticides, *ACS Appl. Mater. Interfaces*, 2023, **15**(16), 20385–20397, DOI: 10.1021/acsami.3c00849.

69 M. L. R. Del Castillo, E. López-Tobar, S. Sanchez-Cortes, G. Flores and G. P. Blanch, Stabilization of curcumin against photodegradation by encapsulation in gamma-cyclodextrin: A study based on chromatographic and spectroscopic (Raman and UV–visible) data, *Vib. Spectrosc.*, 2015, **81**, 106–111, DOI: 10.1016/j.vibspec.2015.10.008.

70 C. Ispas, D. Andreescu, A. Patel, D. V. Goia, S. Andreescu and K. N. Wallace, Toxicity and developmental defects of different sizes and shape nickel nanoparticles in zebrafish,

Environ. Sci. Technol., 2009, **43**(16), 6349–6356, DOI: **10.1021/es9010543**.

71 M. V. D. Z. Park, A. M. Neigh, J. P. Vermeulen, L. J. J. De La Fonteyne, H. W. Verharen, J. J. Briedé, *et al.*, The effect of particle size on the cytotoxicity, inflammation, developmental toxicity and genotoxicity of silver nanoparticles, *Biomaterials*, 2011, **32**(36), 9810–9817, DOI: **10.1016/j.biomaterials.2011.08.085**.

72 S. Selvaraj, M. Perera, P. Yapa, I. Munaweera, I. C. Perera, T. Senapathi, *et al.*, In vitro Analysis of XLAsp-P2 Peptide Loaded Cellulose Acetate Nanofiber for Wound Healing, *J. Pharm. Sci.*, 2025, **114**(2), 911–922, DOI: **10.1016/j.xphs.2024.10.050**.

73 A. Megalathan, S. Kumarage, A. Dilhari, M. M. Weerasekera, S. Samarasinghe and N. Kottegoda, Natural curcuminoids encapsulated in layered double hydroxides: a novel antimicrobial nanohybrid, *Chem. Cent. J.*, 2016, **10**(1), 35, DOI: **10.1186/s13065-016-0179-7**.

74 P. Yapa, I. Munaweera, M. M. Weerasekera, L. Weerasinghe and C. Sandaruwan, Potential antifungal applications of heterometallic silica nanohybrids: A synergistic activity, *Biomater. Adv.*, 2024, **162**(213930), 213930, DOI: **10.1016/j.bioadv.2024.213930**.

75 I. Munaweera and P. Yapa, *Principles and Applications of Nanotherapeutics*, Taylor & Francis, London, England, 2024.

76 P. Mosallanezhad, H. Nazockdast, Z. Ahmadi and A. Rostami, Fabrication and characterization of polycaprolactone/chitosan nanofibers containing antibacterial agents of curcumin and ZnO nanoparticles for use as wound dressing, *Front. Bioeng. Biotechnol.*, 2022, **10**, DOI: **10.3389/fbioe.2022.1027351**.

77 R. Sedghi, A. Shaabani, Z. Mohammadi, F. Y. Samadi and E. Isaei, Biocompatible electrospinning chitosan nanofibers: A novel delivery system with superior local cancer therapy, *Carbohydr. Polym.*, 2016, **159**, 1–10, DOI: **10.1016/j.carbpol.2016.12.011**.

78 M. Ranjbar-Mohammadi, S. Rabbani, S. H. Bahrami, M. T. Joghataei and F. Moayer, Antibacterial performance and in vivo diabetic wound healing of curcumin loaded gum tragacanth/poly(ε-caprolactone) electrospun nanofibers, *Mater. Sci. Eng., C*, 2016, **69**, 1183–1191, DOI: **10.1016/j.msec.2016.08.032**.

79 A. U. R. Khan, K. Huang, Z. Jinzhong, T. Zhu, Y. Morsi, A. Aldalbahi, M. El-Newehy, X. Yan and X. Mo, Exploration of the antibacterial and wound healing potential of a PLGA/silk fibroin based electrospun membrane loaded with zinc oxide nanoparticles, *J. Mater. Chem. B*, 2021, **9**(5), 1452–1465, DOI: **10.1039/d0tb02822c**.